PATTERN RECOGNITION OF SURFACE ELECTROMYOGRAPHY SIGNALS FOR REAL-TIME CONTROL OF WRIST EXOSKELETONS

by

Zeeshan Omer Khokhar
B.Sc, University of Engineering & Technology, Lahore, 2006

THESIS SUBMITTED IN PARTIAL FULFILLMENT OF
THE REQUIREMENTS FOR THE DEGREE OF

MASTER OF APPLIED SCIENCE

In the
School of Engineering Science

SIMON FRASER UNIVERSITY

Summer 2010

APPROVAL

Name: **Zeeshan Omer Khokhar**

Degree: **M.A.Sc**

Title of Thesis: **Pattern Recognition of Surface Electromyography Signals for Real-Time Control of Wrist Exoskeletons**

Examining Committee:

Chair: **Dr. Edward Park**
Associate Professor, School of Engineering Science

Dr. Carlo Menon
Senior Supervisor
Assistant Professor, School of Engineering Science

Dr. Stephen Robinovitch
Supervisor
Associate Professor, School of Engineering Science

Dr. Mirza Faisal Beg
Internal Examiner
Professor, School of Engineering Science

Date Defended/Approved: 17-June-2010

Declaration of
Partial Copyright Licence

SFU SIMON FRASER UNIVERSITY
THINKING OF THE WORLD

STATEMENT OF ETHICS APPROVAL

The author, whose name appears on the title page of this work, has obtained, for the research described in this work, either:

(a) Human research ethics approval from the Simon Fraser University Office of Research Ethics,

or

(b) Advance approval of the animal care protocol from the University Animal Care Committee of Simon Fraser University;

or has conducted the research

(c) as a co-investigator, collaborator or research assistant in a research project approved in advance,

or

(d) as a member of a course approved in advance for minimal risk human research, by the Office of Research Ethics.

A copy of the approval letter has been filed at the Theses Office of the University Library at the time of submission of this thesis or project.

The original application for approval and letter of approval are filed with the relevant offices. Inquiries may be directed to those authorities.

Simon Fraser University Library
Simon Fraser University
Burnaby, BC, Canada

Last update: Spring 2010

ABSTRACT

Surface electromyography (sEMG) signals have been used in numerous studies for the classification of hand gestures and successfully implemented in the position control of different prosthetic hands. An estimation of the intended torque of the user could also provide sufficient information for an effective force control of hand prosthesis or an assistive device. This thesis presents the use of pattern recognition to estimate the torque applied by a human wrist and its real-time implementation to control an exoskeleton prototype that can function as an assistive device. Data from eight volunteers was gathered and Support Vector Machines (SVM) was used for classification. An average testing accuracy of 88% was achieved for nineteen classes. The classification and control algorithm implemented was executed in less than 125 ms. The results of this study showed that real-time classification of sEMG using SVM for controlling an exoskeleton is feasible.

Keywords: surface electromyography (sEMG); assistive device; pattern recognition; support vector machines (SVM).

Dedicated to my Parents

ACKNOWLEDGEMENTS

I would like to thank my senior supervisor, Dr. Carlo Menon for all his guidance and support without which this dissertation would not have been possible. I would also like to acknowledge all the members of my examining committee for their valuable comments and suggestions. I am also grateful to the administration staff of SFU specially Sandra and Raj for their help.

My deepest regards to my family for all their love and support. My loving mother, who instilled a sense of competition in me, believed in me and whose prayers always got me through. My late father, who promoted my curiosity, taught me to understand the principals and whose insightful nature inspired me to choose the engineering profession. My brother Dr. Salman and my sister Amna with whom I cherish my childhood. And finally my fiancé Nida for making my future look beautiful.

I would also like to thank all the members of the MENRVA research group specially Amirreza, Cormac, Mojgan, Yasong and Zhen, all my friends at SFU including Naeem, Saad, Omar, Munsub and specially my roommate Arshad. You all have made my stay at SFU a memorable era of my life.

TABLE OF CONTENTS

LIST OF FIGURES

LIST OF TABLES

CHAPTER 1 INTRODUCTION

1.1 Motivation

The human hand is the most used part of our musculoskeletal system and hence it needs to be kept strong with exercise and appropriate use. With increasing age, the skeletal muscles tend to lose their strength reducing the autonomy of the seniors. This phenomenon is known as sarcopenia, more commonly known as frailty, and is identified as one of the most important topics in aging [1]. The decline in muscle strength is attributed to multiple neuromuscular factors that include: reduction in number of motor neurons innervating each muscle; decrease in strength of each motor unit; and, loss of muscle mass [2, 3]. Furthermore, declines in motor unit firing rate decreases force output [4]. The decline and unsteadiness in force output is further complicated by osteoporosis, changes in strength of ligaments and tendons, arthritis, and other age-related changes in the musculotendinous system. Although simple mechanical assistive devices are available for force amplification, their performances are unsatisfactory; none are capable of improving functionality of the hand through exercise during the assistive process.

Morley further investigated frailty in detail [5]. First, it is suggested that seniors could prevent frailty by maintaining their autonomy. Second, it is apparent that muscular exercise is the major solution to reverse frailty and its consequences. The functional decline of the hands with aging can possibly be

prevented by training [6], and in particular, by resistance training of hand muscles [7]. In addition, Carmeli et al. [6] note that training should be appropriate such that muscle damage or overexertion does not occur. Prevention of injuries is important in general and specially during exercising. Tendon ruptures of the hand, for instance, are common injuries in seniors [8-10].

Loss of autonomy can also be a consequence of other motor function disorders due to stroke, arthritis, spinal cord injury (SCI) or bone fracture. Such conditions can cause difficulties in activities of daily living (ADL). There is a significant part of population with motor function disabilities. For example the heart and stroke foundation of Canada reports that around 300,000 Canadians are living with effects of stroke and more than 50,000 Canadians suffer from stroke each year [11].

Rehabilitation therapy is normally used on individuals with motor disabilities in order for them to regain their motor abilities. Such therapy is usually provided in acute care hospitals or rehabilitation centers and requires a frequency of about once or twice every week and can continue for several months. This therapy has to be a one-to-one interaction making it very costly. Also, traditional therapy methods lack quantitative assessment of the patient's performance [12]. For these reasons many laboratories involved in bioengineering have developed robotic structures for automatic rehabilitation.

A device can possibly be developed that can serve the purpose of rehabilitation as well as assistance. The device should be portable, light-weight, comfortable and economically affordable. Electromyography (EMG) signals

measures the activity of the muscles and provides important information regarding the neuromuscular disorders [18]. EMG signals can provide information regarding hand functions [17] which can be used for evaluating the response of a person to the therapy. The EMG signals can also be used to identify the intention of the user through the use of different pattern recognition techniques. Therefore, EMG signals could be employed in the device for both rehabilitative as well as assistive mode.

In assistive mode, the seniors will be able to daily use the proposed device and preserve their autonomy in domestic environments. The device, controlled by electromyography (EMG) signals can amplify the force exerted by the hand. The human/machine interface can be designed such that subjects activate their muscles optimally while their force is being amplified. Hence, the device could not just be assistive; it can also train the muscles of the subjects. The device can therefore have three main functions in this mode, namely force amplification (to preserve autonomy), maintaining hand functions (training muscle) and avoiding overexertion (injury prevention).

The proposed device can be operated in rehabilitation mode in which it can provide basic rehabilitation exercises and record the EMG signals for analyzing the response of the patient. As the device is portable, the patients can use it at their homes for longer periods of time. The EMG data recorded from the patient could be sent wirelessly to a physiotherapist through the internet, who can then make changes to the exercises for effective response to therapy. This

technique can greatly reduce the costs of rehabilitation and availability of therapy in remote locations.

1.2 Objective

The design of a rehabilitation/assistive-training device requires a deep understanding of the physiology and functions of the hand; there are 11 intrinsic and 15 extrinsic muscles that control movement and force production. Advances in the technology have made such a device feasible to realize.

The main focus of this thesis was on the development of a real-time surface EMG (sEMG) pattern recognition system for the movement of the wrist, in terms of both force and direction, that can be used in assistive devices or advanced hand prosthetics. Different control strategies for exoskeleton prototypes were also developed and tested in real-time. Many researchers have worked on pattern recognition to predict hand gestures using sEMG signals but have not considered the amount of force applied by the user, which is a basic requirement for the development of an assistive device. In the current study, isometric measurements were taken for the wrist torque meaning that there was no actual movement of the wrist. In practical application, such a condition occurs when a person is not able to move his wrist due to lack of torque for example when trying to open a tight jar or opening a tight screw. An assistive device using the proposed system can potentially work in such scenarios where there is no movement of the wrist or the movement is so slow that it does not affect the system performance.

In particular, sEMG signals along with the torque applied by the wrist was collected from eight volunteers during isometric measurements. The data was divided into two groups with nineteen and thirteen classes and then Support Vector Machines (SVM) was used for their classification. After verification of the classification system, control strategies for wrist exoskeletons were developed and the whole system was implemented in real-time. Some experiments were also performed to prove the feasibility of using such a technique for an assistive device. In summary the objectives of this thesis were as follows:

a) To identify the forearm muscles that can be used for predicting wrist torque.

b) To extract suitable features from sEMG of the forearm muscles for classification in terms of both direction and force.

c) To gather experimental data for verification of the classification methodology.

d) To implement the classification system and control algorithm for a wrist exoskeleton in real-time.

e) To provide a proof-of-concept for an assistive device using the proposed classification and control system.

1.3 Structure of Thesis

The motivation and objective for this thesis have been discussed. The remaining chapters of the thesis are organized as follows:

Chapter 2 presents a background for the sEMG signals and its applications along with a brief overview of the literature related to different techniques of sEMG pattern recognition and some robotic structures for rehabilitation and prosthetic applications.

Chapter 3 presents the basic techniques of sEMG feature extraction and classification used in this thesis work. It starts with the description of the sEMG data acquisition system used and the protocol followed to acquire data from eight volunteers. The techniques used for feature extraction and classification are presented followed by the results obtained from the study.

Chapter 4 describes the hardware electronic design and implementation used for different exoskeleton prototypes developed by the MENRVA research group to support the thesis work. The development of the position and force control philosophies along with their implementations are described. Also some experiments for the verification of the control strategies were performed and their results are presented.

Chapter 5 brings the classification system and the developed hardware together to form a real-time classification and control system. It presents the detailed application development procedure, the setup for the testing of the system and its results.

Chapter 6 presents a proof-of-concept for an assistive device using the developed real-time system. The setup used for the proof and its results are described in this chapter.

Chapter 7 concludes the thesis work and presents a discussion of the possible future work.

CHAPTER 2 BACKGROUND

2.1 Electromyography (EMG)

The human brain generates commands to control the contractions and relaxation of the muscles through neurons which are responsible for different movements by the human skeletal system. Such control commands are carried through the nervous system which generates an electrical activity in the muscles. An electromyograph detects the electrical potential generated by muscle cells to produce a record, called an electromyogram, when these cells are mechanically active and also when the cells are at rest. Electromyography (EMG) is a technique for evaluating and recording these electromyograms. Thus, EMG signal is a complex biomedical signal controlled by the nervous system and anatomical and physiological properties of the muscles [17]. An example of a simple EMG signal obtained from Flexor Carpi Ulnaris (FCU) muscle during flexion is shown in Figure 2-1.

Francesco Redi first documented the electric potential of muscles using an electric ray fish as early as 1666. In 1849, Dubious Raymond discovered that electric potential of muscles can also be observed during voluntary muscle contractions. The term EMG was introduced by Marey in 1890 who took the first actual reading of the electric potential during muscle contraction.

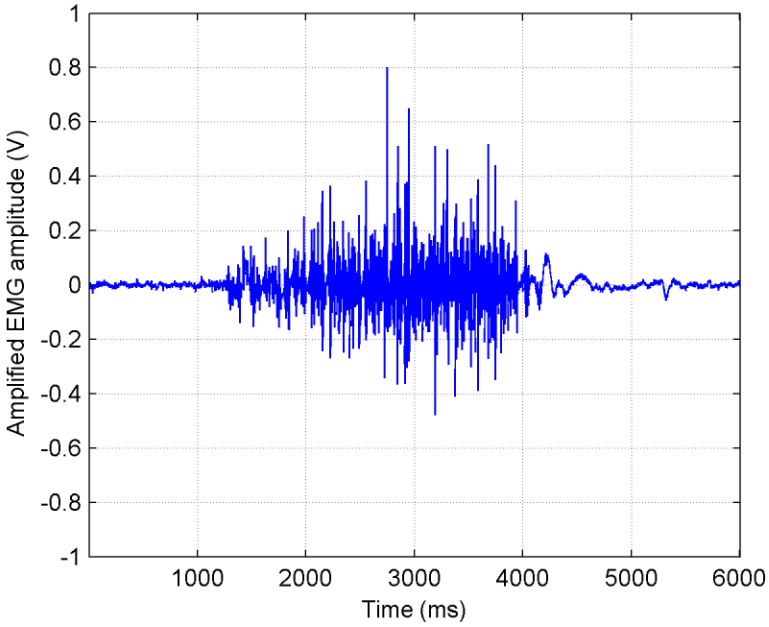

Figure 2-1: An example of an EMG signal

2.2 Techniques for EMG

There are two major techniques for EMG; needle EMG and surface EMG (sEMG). In needle EMG, the electrodes in the form of a needle or thin wires is placed invasively into the muscle and the signal is acquired. The needle used is normally as slim as 25 gauge and produce a minor discomfort that a patient can normally tolerate. Needle EMG are normally used in clinical settings and can be used to diagnose abnormalities such as carpal tunnel syndrome, ulnar neuropathy, peripheral neuropathy, cervical and lumber radiculopathy. The skills of the examiner play an important role in needle EMG and the tests need to be tailored for the patient's particular clinical problem.

In sEMG, the electrodes are placed on the skin noninvasively above the muscle. The ease of signal acquisition makes sEMG very popular however there are some issues with sEMG signal acquisition. The amplitude of the sEMG signals lie in the range of 0-10 mV peak to peak making them susceptible to all sorts of noise making it difficult to acquire a clean signal. The major sources of noise in sEMG signal acquisition, as indicated by Reaz [17], are inherent noise in the electronic equipment, ambient noise due to different sorts of radiation in the surrounding atmosphere, motion artefacts at the electrode interface and electrode cables and finally the inherent instability of signals due to the random nature of sEMG signals.

2.3 Applications of sEMG

sEMG can provide information regarding the neural activation of muscles, which can be used to estimate the intention of the person and also identify potential neuromuscular disorders [17]. The use of sEMG signals has been explored for different applications. Man-machine interface can use sEMG to connect a person directly to a computer to substitute for joysticks and keyboards using gestures [60]. People without vocal cards can use sEMG of the muscles associated with speech to recognize unvoiced speech [61]. sEMG can also be used to control mobile robots [62] and wheelchairs. There are also many more applications for sEMG and two of these, which are related to the thesis work, are presented in some detail.

2.3.1 Rehabilitation through robotic devices

One of the applications of sEMG signals is in regards to rehabilitation through robotic devices. Rehabilitation therapy is normally provided in acute care hospitals or rehabilitation centres and is normally a one-to-one interaction making it very costly. Traditional therapy methods also lack quantitative assessment of the patients hand and therefore many researchers have developed robotic structures for rehabilitation. One of these includes a therapy joystick developed at the center for biomedical engineering at the University of California [13]. The commercial joystick used in this therapy is able to assist or resist the movement of the person based on the therapy requirement. It can also provide quantitative feedback of movement performance through the web to assess rehabilitation progress. A picture of a person using the joystick is shown in Figure 2-2.

Figure 2-2: Therapy Joystick. Reproduced from [13]

A wrist rehabilitation robot was developed in the Newman Laboratory for biomechanics and human rehabilitation at MIT [14]. This robot was designed specifically for the wrist and was not designed for portability. This robot was designed to be used in clinical setup for performing rehabilitative exercises. A picture of the device at different postures is shown in Figure 2-3.

Figure 2-3: A wrist rehabilitation robot. Reproduced from [14]

A hand rehabilitation device was also developed at the Electronic and Information Department, Politecnico di Milano [15]. This hand robot was portable

and was specifically designed to be used by persons who have partially lost the ability to move their hand musculature. This robot used the EMG signals to identify the intention of the user and provide assistive force for the movement. As such the purpose was to improve the autonomy of the user while providing rehabilitation therapy. A picture of this robot is shown in Figure 2-4. The experiments done with this robot only consisted of finger movements and not of the wrist.

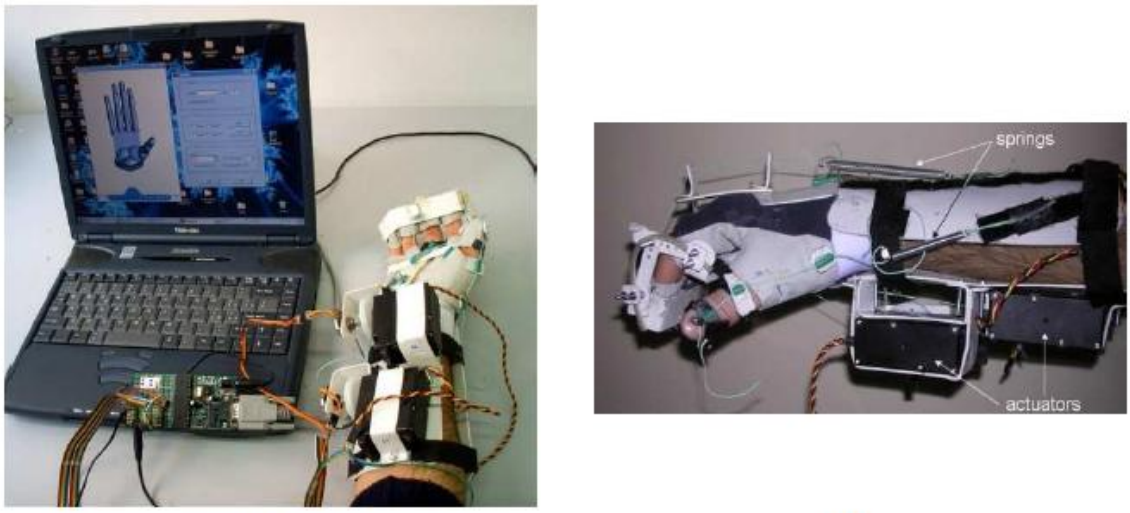

Figure 2-4: A hand rehabilitation robot. Reproduced from [15]
(a) Overview of complete system, (b) Lateral view of exoskeleton

Another robot for hand rehabilitation was developed in the Department of Mechanical Engineering at the University of Victoria [16]. This portable robot was capable of independently flexing/extending the metcarpophalangeal (MCP) and proximal interphalangeal (PIP) joints from 0º to 90º so that typical hand rehabilitation motions, such as intrinsic plus, intrinsic minus and a fist, could be

achieved. This robot was capable of both active and passive motions. A picture of this robot is shown in Figure 2-5.

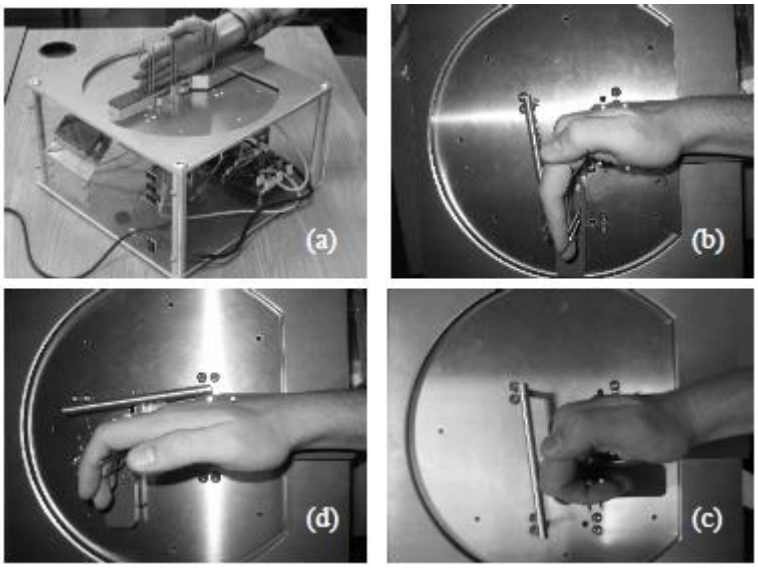

Figure 2-5: Hand rehabilitation robot prototype. Reproduced by [16]
(a) initial position, (b) intrinsic plus at MCP, (c) fist, (d)intrinsic minus at PIP

It has been proposed that sEMG signals can be used to quantify the assessment of hand functions [18] and robotic devices can be used to provide an assistive force as a compensation for hand movement [19]. Combining sEMG signals with robotic therapy can optimize the coordination of motor commands and actual movement [20-22].

2.3.2 Control of prosthetic hands

Another application of EMG signals is in the control of prosthetic hands. Numerous prosthetic hands have been prototyped and some have also been commercialized. In these research and development efforts, the goal was to

obtain a lightweight and dexterous prosthetic hand that could perform movements similar to a human hand. A crucial aspect towards an effective use of these prosthetic hands is their intuitive control, which could be achieved through detection and interpretation of the user's neurological activity to be detected, for example, through sEMG electrodes.

One of the prototyped prosthetic hand is the CyberHand [23] shown in Figure 2-6. CyberHand is an under actuated prosthetic with 16 degree of freedom and is capable of exerting a grasping force of 40 N. It uses DC motors and weighs around 450 grams.

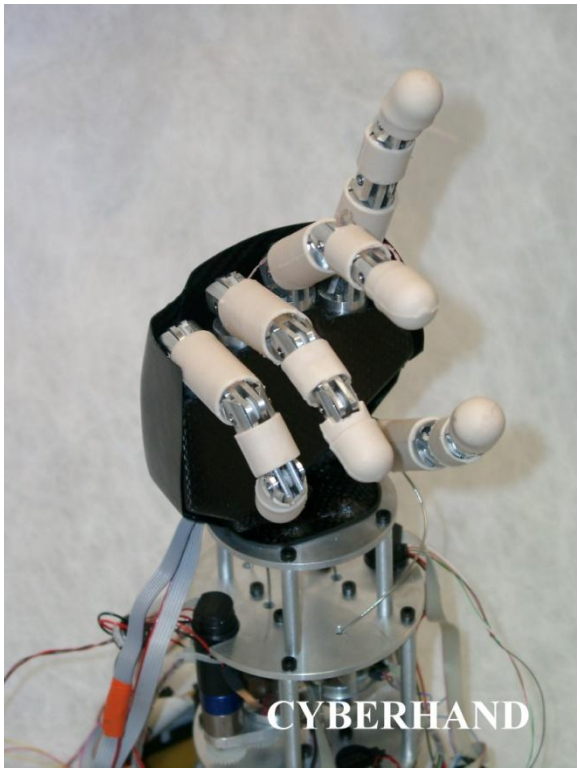

Figure 2-6: CyberHand prosthetic prototype. Reproduced from [23]

Another prototype prosthetic is the SmartHand [24] shown in Figure 2-7. The purpose of this prosthetic hand project is to improve mobility and diminish phantom pains associated with amputees.

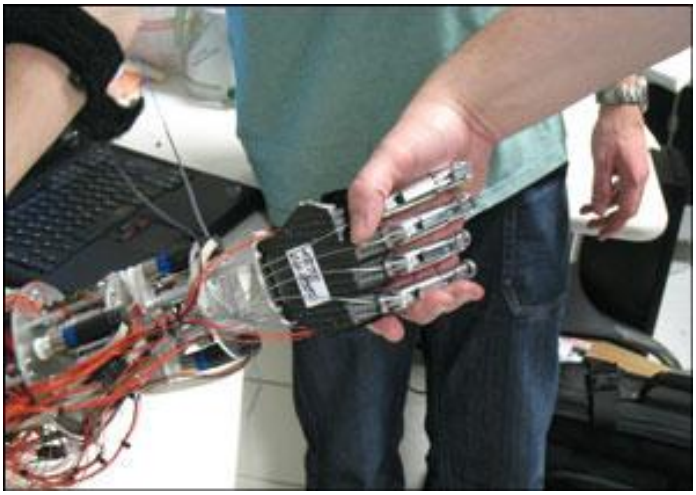

Figure 2-7: SmarHand prosthetic prototype. Reproduced from [24]

Among the commercially available prosthetic hands are the iLimb [25] (shown in Figure 2-8) and the Otto Bock's Transcarpal Hand [26] (shown in Figure 2-9). These prosthetic hands take input from the sEMG signals of the user to control the movement but are only capable of performing very basic actions without any fine control over the individual joints. From the comparison of the prototyped and commercial prosthetic hands, it is apparent that the main issue is to achieve input signals for the control and not a mechanical structure that can imitate a human hand.

Figure 2-8: iLimb Prosthetic Hand. Reproduced from [25]

(a) iLimb Hand, (b) iLimb Pulse

Figure 2-9: Ottobock transcarpal hand prosthetic. Reproduced from [26]

2.4 Pattern recognition of sEMG signals

Whether used for controlling an assistive, rehabilitative or prosthetic device, the basic challenge is to be able to process sEMG signals and identify the intention of the user. Different studies have been performed to tackle this

challenge by using different pattern recognition methods [27-44]. The analysis of pattern recognition in sEMG mainly consists of two steps, namely feature extraction and classification. Feature extraction is the dimensionality reduction of the raw sEMG input to form a feature vector - the accuracy of the pattern classification system almost entirely depends on the choice of these features [27]. Features cannot be extracted from the individual samples as the structural detail of the signal will be lost and hence the features need to be calculated by segmenting the raw sEMG signal and calculating a set of features from each segment [27]. Researchers have experimented with the length of the segment and the constraint in the length mainly derives from the specific real-time implementation. A delay of 200~300 ms interval is the clinically recognized maximum delay tolerated by the users [45]. A suitable delay for the controller to generate a control command should therefore be between 100~125 ms [46]. Different features have been used in pattern recognition involving both time domain and time-frequency domain features. Some of these include mean absolute value [27,28,31-33], zero crossings (ZC) [27,28,31-33], slope sign changes (SSC) [27,28,31,32], autoregressive (AR) model coefficients [28,31,34-36], cepstrum coefficients [35], waveform length (WL) [27,28,32,33] and wavelet packet transform[29-31]. As regards to classification, it can be defined as the process of assigning one of K discrete classes to an input vector $\boldsymbol{x}$ [56]. Numerous studies have been done to classify the features extracted from the sEMG like neural networks [27,36,37], bayesian classifier [40], linear discriminant analysis [32,39], hidden markov model [42], multilayer perceptron [29,30,39],

fuzzy classifier [31,33-35], gaussian mixture model [28] and support vector machines (SVM) [37,38,43,44].

Feature extraction and classification methods were primarily used in previous research studies to identify the orientation of the hand without considering the amount of force the user was applying. In the use of advanced hand prostheses, it would however be beneficial having control over the amount of force a person intends to apply and, for assistive devices, force control would indeed be necessary. Castellini *et al.* [37] successfully controlled the amount of force applied by the fingers in different types of grasp so that the user could apply a different amount of force for holding, for example, a hammer or an egg [37].

CHAPTER 3 PROPOSED FEATURE EXTRACTION AND CLASSIFICATION SCHEME

The major task in realizing the objectives, described in chapter 1, is to be able to identify the intention of the user. Classification techniques have been successfully utilized for processing bio-signals and therefore seems suitable for our application. This chapter proposes a classification scheme and describes the data collection procedures, feature extraction techniques and classification results obtained.

3.1 sEMG Data Acquisition

Several forearm muscles contribute to the movement of the wrist, details of which can be found in [47]. Four forearm muscles were identified as suitable candidates for classification of wrist torques through a trade-off experimental procedure. The four selected muscles were Flexor Carpi Ulnaris (FCU), Palmaris Longus (PL), Extensor Digitorum (ED) and Extensor Carpi Radialis (ECR). FCU assists in wrist flexion with ulnar deviation, PL assists in wrist flexion, ED assists in extension of four fingers and aids in extension of the wrist and ECR assists in extension and radial abduction of the wrist. The approximate position of these muscles is shown in Figure 3-1.

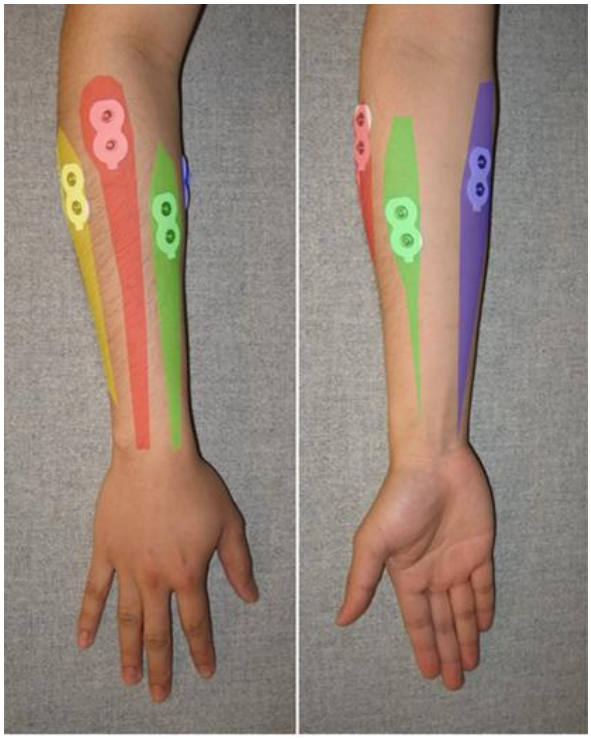

Figure 3-1: Position of muscles of the forearm

ED is shown in red, ECR in yellow, PL in green and FCU in purple color

Reliable sEMG data acquisition is necessary before extracting features for classification. Numerous factors affect the quality of sEMG acquisition such as inherent noise in the electronic equipment, ambient noise in the surrounding atmosphere, motion artefacts and poor contact with skin. The first three factors are dependent on the sEMG acquisition system used and, to reduce the effects of these, a commercial sEMG system from Noraxon (Myosystem 1400L) was used. In order to have a good skin contact with the electrodes, the guidelines of the surface electromyography for the non-invasive assessment of muscles (SENIAM) project [48] were followed. The skin of the volunteer was shaved and

an alcohol swab was used to clean the skin. The electrodes were placed at the desired locations after the skin dried. AgCl gel dual electrodes from Noraxon were used, which contains two electrodes at a recommended distance. The acquired sEMG signal was then digitized at 1024 samples per second using a data acquisition card from National Instruments (NI USB-6289) and stored on a computer by the LabVIEW software.

3.2 Data Collection Protocol

A total of eight volunteers participated in the current study. Two testing rigs were built to record the direction and level of torque applied by the wrist. The first rig was designed to record the level of torque for flexion/extension of the wrist (see Figure 3-2-a) and the second rig to record the level of torque for ulnar/radial deviation of the wrist (see Figure 3-2-b). Both rigs consisted of two separate sheets of aluminium connected together with a reaction torque sensor (Transducer Techniques TRT-100). The forearm rested on one plate and the hand rested on the second such that the torque sensor read the torque produced at the wrist joint. An application was developed using LabVIEW software to simultaneously acquire both the sEMG signals and the torque readings. Each volunteer followed the twelve protocols summarized in Table 3-1. Protocols 1, 2, 5 and 6 were used to record the maximum torque produced by the user in each direction and this was designated as the maximum voluntary contraction (MVC). A visual bar graph was represented on the screen of a monitor to provide a visual feedback of the produced wrist torque in real-time – this feature was needed especially to complete protocols 3, 4, 7 and 8, which were used to generate data

for the formation of the classes. All the protocols listed in Table 3-1 never exceeds 50% of the MVC because studies have shown that in order to avoid upper extremity musculoskeletal injuries force should not exceed 40-50% of the maximum [49].

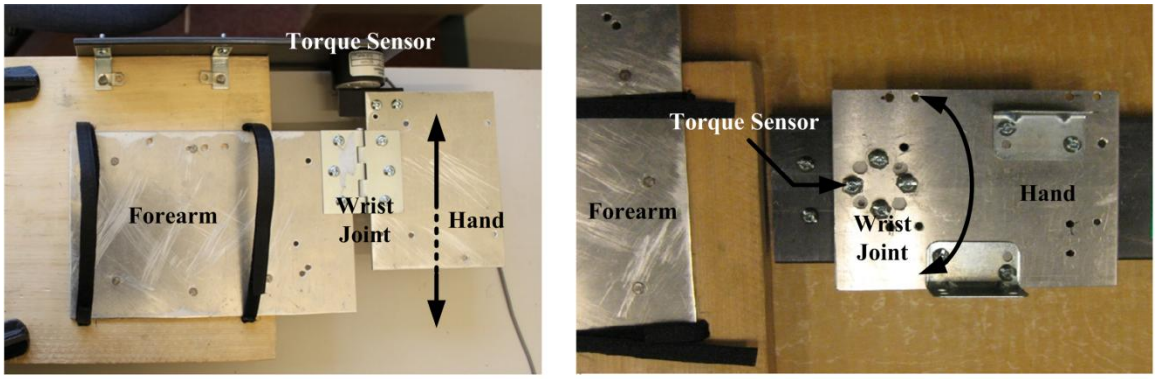

Figure 3-2: Testing rigs to measure wrist torque

(a) Rig to measure torque during wrist flexion/extension; and (b) Rig to measure torque during wrist ulnar/radial deviation

Table 3-1: Protocol Information

Protocol Number	Action	Number of Repetition
1	Wrist flexion with maximum torque	3
2	Wrist extension with maximum torque	3
3	Wrist flexion: start from rest and increase torque by 10% of MVC after every 10 seconds until 50% of MVC is applied	3
4	Wrist flexion: start from 50% of MVC and decrease torque by 10% after every 10 seconds until no torque is applied	3
5	Wrist extension: start from rest and increase torque by 10% of MVC after every 10 seconds until 50% of MVC is applied	3
6	Wrist extension: start from 50% of MVC and decrease torque by 10% after every 10 seconds until no torque is applied	3
7	Wrist ulnar deviation with maximum torque	3
8	Wrist radial deviation with maximum torque	3
9	Wrist ulnar deviation: start from rest and increase torque by 10% of MVC after every 10 seconds until 40% of MVC is applied	3
10	Wrist ulnar deviation: start from 40% of MVC and decrease torque by 10% after every 10 seconds until no torque is applied	3
11	Wrist radial deviation: start from rest and increase torque by 10% of MVC after every 10 seconds until 40% of MVC is applied	3
12	Wrist radial deviation: start from 40% of MVC and decrease torque by 10% after every 10 seconds until no torque is applied	3

3.3 Feature Extraction

After the data collection, the acquired samples were converted into features that could be used for classification. Matlab software was used to extract and classify the features using the recorded sEMG signals. Features were extracted from the samples by segmenting the signal into 250 ms intervals corresponding to 256 samples in each segment. A single feature was calculated

from each segment and the segment window was incremented by 125 ms (128 samples) for the next feature. This scheme ensured that a control command could be generated within 250 ms from the instant the user's intention was given. Three kinds of features were extracted from each segment namely EMG rms value, AR model coefficients and WL.

3.3.1 rms Values

The EMG rms value, r_k, is computed as:

$$r_k = \sqrt{\frac{\sum_{i=1}^{N} x_i^2}{N}} \tag{2-1}$$

where x_i is the value of the i^{th} sample in the k^{th} segment and N is the number of samples, which in our case is 256.

3.3.2 Autoregressive Model Coefficients

AR models are constructed using a recursive filter. This filter predicts the current value based on the previous output values of the filter. The current value $y(t)$ can be computed as:

$$y(t) = \sum_{i=1}^{m} a_i y(t-i) + \varepsilon(t) \tag{2-2}$$

where a_i are the model coefficients, m is the order of the model and ε is the output error. AR model coefficients were used as the features with a model order of four, which is adequate for modelling EMG signals [50], thus generating four features for each channel of sEMG.

3.3.3 Waveform Length

The third kind of extracted feature was the waveform length, which provided a measure of the waveform complexity in each segment. The waveform length *l* can be mathematically represented as:

$$l = \sum_{k-1}^{N} |\Delta x_k| = \sum_{k-1}^{N} |x_k - x_{k-1}| \tag{2-3}$$

Four channels of sEMG data were used, which therefore provided 24 features per segment.

3.4 Classification using Support Vector Machines

Classification was done using Support Vector Machines (SVM) utilizing the LibSVM tool [51] in the Matlab environment (a brief description of SVM can be found in Appendix A). LibSVM has an implementation for multi class SVM using one-versus-one strategy. The following radial basis function (RBF) was selected as a kernel in the SVM:

$$K(x_i, x_j) = \exp(-\gamma \left\| x_i - x_j \right\|^2), \qquad \gamma > 0 \tag{2-4}$$

The choice of radial basis function is based on the fact that RBF nonlinearly maps samples into higher dimensional space which means that it would be efficient in classifying nonlinear data. Furthermore, RBF has lower model complexity and fewer hyper parameters than most other kernels. RBF is ideally suited for cases where the number of features is not very large with nonlinear data, as is the case with sEMG signal classification.

To determine the value of the parameters for a kernel, cross validation is normally used along with grid search. In a *v*-fold cross-validation, a data set is divided into *v* groups of equal size. A group is sequentially left out while the rest of the data is used to train the classifier. The accuracy of the classifier is then tested on the left out group. This process is continued such that each group of the whole training data set is predicted once and the cross validation accuracy is the average of all the testing accuracies achieved. Thus cross-validation accuracy is the percentage of data which are correctly classified. In this study, eight fold cross validation along with grid search was used to find the optimal parameters for *C* and γ. Different pairs of (C, γ) were tried for cross validation and the one with highest accuracy was chosen. The process was started with a course grid search and after identifying a region of better accuracy, fine grid search was performed on that region. The process of using grid search with cross validation on volunteer # 02 is shown in Figure 3-3, 3-4 and 3-5. Figure 3-3 shows the results of course grid search where C varies from 2^1 to 2^8 and γ varies from 2^{-4} to 2^2 with an exponential step size in consecutive powers of 2. A region for better accuracy was identified near C=2^6 and γ=2^1 and a finer grid search is performed where C varies from 20 to 100 with a step size of 10 and γ varies from 0.5 to 3.1 with a step size of 0.2 as shown in Figure 3-4. The maximum accuracy is at C=100 γ=1.3. Finally, the parameters are chosen by performing a grid search in the region where C varies from 80 to 120 with a step size of 5 and γ varies from 0.9 to 1.7 with a step size of 0.1 as shown in Figure 3-5. The final parameters chosen are C=80 and γ=1.6.

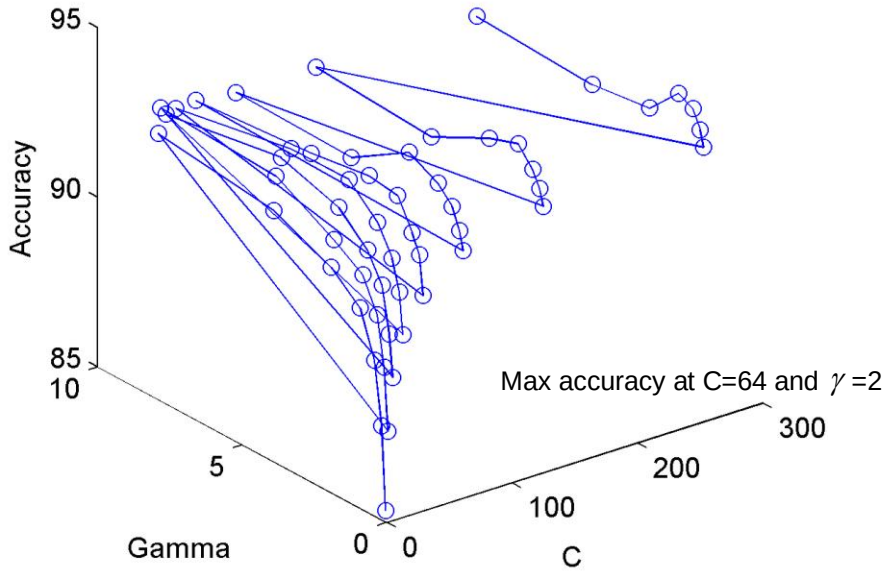

Figure 3-3: Grid search using 8-fold cross validation with C=2^1 to 2^8 and γ =2^{-4} to 2^2

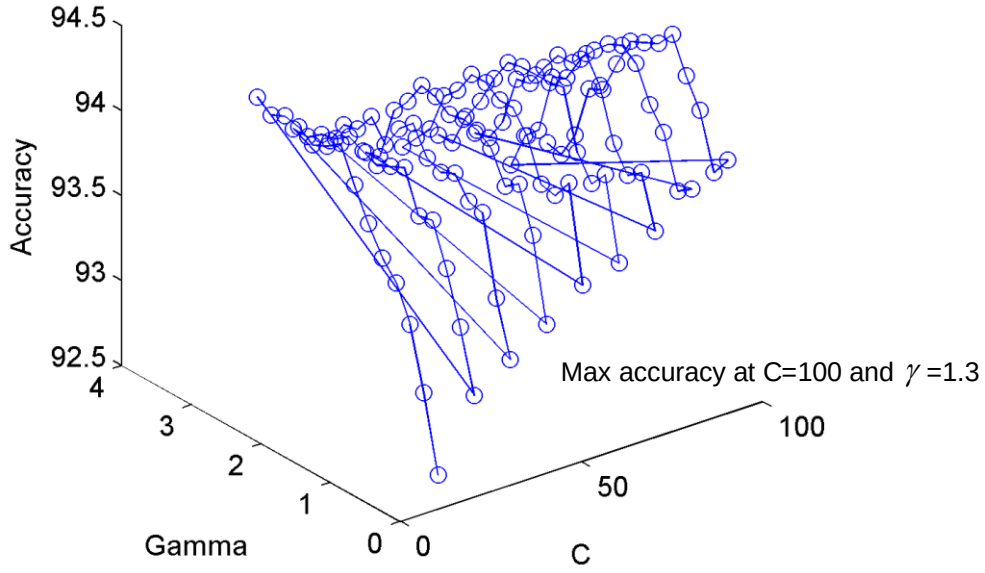

Figure 3-4: Grid search using 8-fold cross validation with C=20 to 100 and γ =0.5 to 3.1

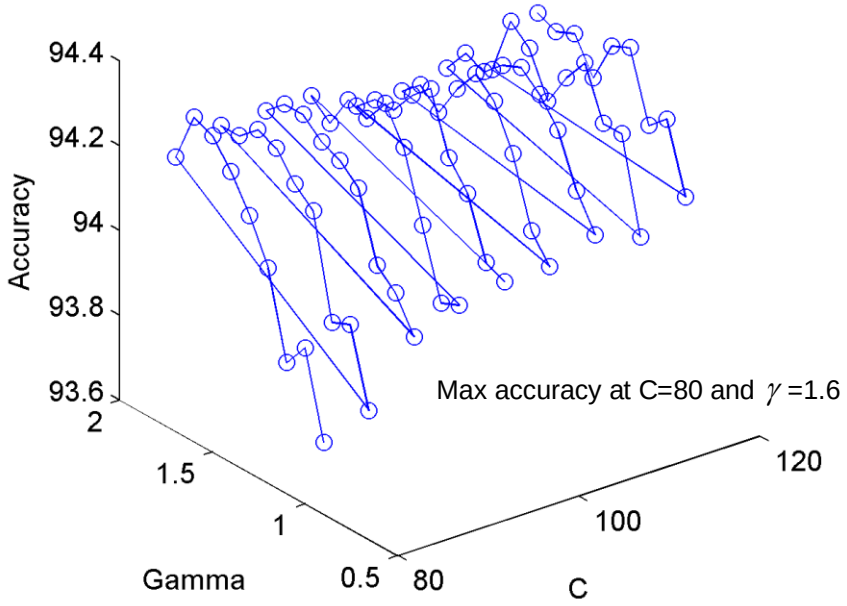

Figure 3-5: Grid search using 8-fold cross validation with C=80 to 120 and γ =0.9 to 1.7

The sEMG data gathered from the volunteers was analyzed in two configurations. The first configuration consisted of nineteen classes and the second one used thirteen classes. The purpose of using two different configurations was to obtain preliminary results enabling a trade-off between the accuracy of the classifier and the smoothness of the torque provided by the assistive device. Six seconds of data per iteration per protocol was extracted for each class, which provided 282 data segments per class and 5358 data segments for 19 classes. Out of these, 4788 data segments were used as training data and 570 data segments were used as testing data. Table 3-2 specifies the 19 classes used for the first configuration. For the second configuration (13 classes), class 3, 5, 8, 10, 13 and 17 were removed. The

division of classes is at particular force level but the SVM classifier works on maximizing the margin between the adjacent classes meaning that in an ideal case, the boundary between two adjacent classes will be exactly in the middle such that a flexion with 15% MVC to 25% MVC will belong to class 3. In practical scenarios these boundary levels may differ based on how accurately the volunteer was able to follow the training protocol.

Table 3-2: Actions for different classes

Class Number	Class Label	Associated action
1	Rt	Resting position
2	F1	Flexion with 10% of MVC torque
3	F2	Flexion with 20% of MVC torque
4	F3	Flexion with 30% of MVC torque
5	F4	Flexion with 40% of MVC torque
6	F5	Flexion with 50% of MVC torque
7	E1	Extension with 10% of MVC torque
8	E2	Extension with 20% of MVC torque
9	E3	Extension with 30% of MVC torque
10	E4	Extension with 40% of MVC torque
11	E5	Extension with 50% of MVC torque
12	U1	Ulnar deviation with 10% of MVC torque
13	U2	Ulnar deviation with 20% of MVC torque
14	U3	Ulnar deviation with 30% of MVC torque
15	U4	Ulnar deviation with 40% of MVC torque
16	R1	Radial deviation with 10% of MVC torque
17	R2	Radial deviation with 20% of MVC torque
18	R3	Radial deviation with 30% of MVC torque
19	R4	Radial deviation with 40% of MVC torque

3.5 Classification Results

As mentioned earlier, the data was analyzed in two configurations. The configuration with 19 classes consisted of a training feature vector of size 4788 x

24. After cross validation and grid search to find the optimal parameters, the prediction was tested by using a test feature vector of size 570 x 24. An average accuracy of 88.2% was observed. Table 3-3 summarizes the results of classification on each individual volunteer.

Table 3-3: Classification results with 19 classes

Volunteers	C	γ	Cross Validation Accuracy (%)	Testing Accuracy (%)
Volunteer # 1	45	1	94.05	90.8621
Volunteer # 2	80	1.6	94.36	92.5
Volunteer # 3	85	1	90.24	85.67
Volunteer # 4	90	0.9	91.94	86.5
Volunteer # 5	75	1	88.77	86
Volunteer # 6	85	1	88.11	84
Volunteer # 7	75	1	90.58	87
Volunteer # 8	90	0.7	94.26	93.57
Mean			91.53875	88.26276
Standard Deviation			2.503149	3.537414

Results obtained for classification accuracy in volunteers who had greater MVC and those who could maintain a torque level with little variation were much better than the rest. Also, most of the errors were due to a class misclassified in an adjacent class as will be seen in section 3.6. The average accuracy for the eight volunteers neglecting misclassification in adjacent classes reached up to 99.99%. This suggests that the cause of lower accuracy is the small separation between torque levels; to evaluate the trade-off between smoothness of torque and average accuracy of the classifier, the second configuration was analyzed.

The second configuration consisted of 13 classes with a training feature vector of size 3276 x 24 and a testing feature vector of size 390 x 24. Using the same 8 fold cross validation and grid search, it was observed that the average accuracy increased to 96.52%. The classification accuracies for individual volunteers are shown in Table 3-4. The accuracy reached 99.47% in the case of the eighth volunteer.

Table 3-4: Classification results with 13 classes

Volunteer	C	γ	Cross Validation Accuracy (%)	Testing Accuracy (%)
Volunteer # 1	50	0.7	99.72	97.95
Volunteer # 2	60	1	98.61	98.57
Volunteer # 3	80	1	98.1	94.76
Volunteer # 4	90	0.9	97.39	94.05
Volunteer # 5	75	1	95.83	94.76
Volunteer # 6	70	1	96.8	96.19
Volunteer # 7	80	0.9	97.71	96.43
Volunteer # 8	90	1	99.58	99.47
Mean			97.97	96.52
Standard Deviation			1.33	1.98

Tables 3-3 and 3-4 show that, as expected, classification accuracy decreased when the number of classes increased but still good results were obtained with the highest number of classes. Depending on the needs of specific future practical applications, which could have different requirements on the smoothness of the output torque of the assistive device or high precision in the identification of the user intention, the number of classes could therefore be selected appropriately and could be between 13 and 19 classes.

3.6 Confusion Matrices

A confusion matrix is a visualization tool to assess the performance of a classifier in a supervised learning method. Each row of this matrix represents the number of samples in the predicted class while each column represents the number of samples in the actual class. For a perfect classification, all the number should appear in the diagonal with zero at every non-diagonal element of the matrix. This matrix is useful to identify if any two classes is being confused by the classifier. The confusion matrices for the best and worst testing accuracy for both 19 classes and 13 classes are presented in Table 3-5 to 3-8.

Table 3-5: Confusion Matrix for Volunteer # 8 with 19 classes

Predicted Class Labels \ Actual Class Labels	Rt	F1	F2	F3	F4	F5	E1	E2	E3	E4	E5	U1	U2	U3	U4	R1	R2	R3	R4
Rt	30	0	0	0	0	0	0	0	0	0	0	0	0	0	0	0	0	0	0
F1	0	29	0	0	0	0	0	0	0	0	0	0	0	0	0	0	0	0	0
F2	0	0	29	2	0	0	0	0	0	0	0	0	0	0	0	0	0	0	0
F3	0	0	1	27	2	0	0	0	0	0	0	0	0	0	0	0	0	0	0
F4	0	0	0	1	25	1	0	0	0	0	0	0	0	0	0	0	0	0	0
F5	0	0	0	0	3	29	0	0	0	0	0	0	0	0	0	0	0	0	0
E1	0	0	0	0	0	0	30	0	0	0	0	0	0	0	0	0	0	0	0
E2	0	0	0	0	0	0	0	30	2	0	0	0	0	0	0	0	0	0	0
E3	0	0	0	0	0	0	0	0	25	7	0	0	0	0	0	0	0	0	0
E4	0	0	0	0	0	0	0	0	3	20	2	0	0	0	0	0	0	0	0
E5	0	0	0	0	0	0	0	0	0	3	28	0	0	0	0	0	0	0	0
U1	0	1	0	0	0	0	0	0	0	0	0	30	0	0	0	0	0	0	0
U2	0	0	0	0	0	0	0	0	0	0	0	0	27	1	0	0	0	0	0
U3	0	0	0	0	0	0	0	0	0	0	0	0	3	29	1	0	0	0	0
U4	0	0	0	0	0	0	0	0	0	0	0	0	0	0	29	0	0	0	0
R1	0	0	0	0	0	0	0	0	0	0	0	0	0	0	0	30	0	0	0
R2	0	0	0	0	0	0	0	0	0	0	0	0	0	0	0	0	28	0	0
R3	0	0	0	0	0	0	0	0	0	0	0	0	0	0	0	0	2	29	0
R4	0	0	0	0	0	0	0	0	0	0	0	0	0	0	0	0	0	1	30

Table 3-6: Confusion Matrix for Volunteer # 6 with 19 classes

Predicted Class Labels \ Actual Class Labels	Rt	F1	F2	F3	F4	F5	E1	E2	E3	E4	E5	U1	U2	U3	U4	R1	R2	R3	R4
Rt	30	0	0	0	0	0	0	0	0	0	0	0	0	0	0	0	0	0	0
F1	0	30	0	0	0	0	0	0	0	0	0	0	0	0	0	0	0	0	0
F2	0	0	26	1	0	0	0	0	0	0	0	0	0	0	0	0	0	0	0
F3	0	0	4	22	1	0	0	0	0	0	0	0	0	0	0	0	0	0	0
F4	0	0	0	7	21	7	0	0	0	0	0	0	0	0	0	0	0	0	0
F5	0	0	0	0	8	23	0	0	0	0	0	0	0	0	0	0	0	0	0
E1	0	0	0	0	0	0	29	6	1	0	0	0	0	0	0	0	0	0	0
E2	0	0	0	0	0	0	1	19	0	0	0	0	0	0	0	0	0	0	0
E3	0	0	0	0	0	0	0	5	29	4	0	0	0	0	0	0	0	0	0
E4	0	0	0	0	0	0	0	0	0	22	4	0	0	0	0	0	0	0	0
E5	0	0	0	0	0	0	0	0	0	4	26	0	0	0	0	0	0	0	0
U1	0	0	0	0	0	0	0	0	0	0	0	19	4	0	0	0	0	0	0
U2	0	0	0	0	0	0	0	0	0	0	0	8	19	8	0	0	0	0	0
U3	0	0	0	0	0	0	0	0	0	0	0	3	7	20	1	0	0	0	0
U4	0	0	0	0	0	0	0	0	0	0	0	0	0	2	29	0	0	0	0
R1	0	0	0	0	0	0	0	0	0	0	0	0	0	0	0	30	0	0	0
R2	0	0	0	0	0	0	0	0	0	0	0	0	0	0	0	0	25	0	0
R3	0	0	0	0	0	0	0	0	0	0	0	0	0	0	0	0	5	25	0
R4	0	0	0	0	0	0	0	0	0	0	0	0	0	0	0	0	0	5	30

Table 3-7: Confusion Matrix for Volunteer # 8 with 13 classes

Predicted Class Labels \ Actual Class Labels	Rt	F1	F3	F5	E1	E3	E5	U1	U3	U4	R1	R3	R4
Rt	30	0	0	0	0	0	0	0	0	0	0	0	0
F1	0	29	0	0	0	0	0	0	0	0	0	0	0
F3	0	0	30	0	0	0	0	0	0	0	0	0	0
F5	0	0	0	30	0	0	0	0	0	0	0	0	0
E1	0	0	0	0	30	0	0	0	0	0	0	0	0
E3	0	0	0	0	0	29	0	0	0	0	0	0	0
E5	0	0	0	0	0	1	30	0	0	0	0	0	0
U1	0	1	0	0	0	0	0	30	0	0	0	0	0
U3	0	0	0	0	0	0	0	0	30	0	0	0	0
U4	0	0	0	0	0	0	0	0	0	30	0	0	0
R1	0	0	0	0	0	0	0	0	0	0	30	0	0
R3	0	0	0	0	0	0	0	0	0	0	0	30	0
R4	0	0	0	0	0	0	0	0	0	0	0	0	30

Table 3-8: Confusion Matrix for Volunteer # 6 with 13 classes

Predicted Class Labels \ Actual Class Labels	Rt	F1	F3	F5	E1	E3	E5	U1	U3	U4	R1	R3	R4
Rt	30	0	0	0	0	0	0	0	0	0	0	0	0
F1	0	30	0	0	0	0	0	0	0	0	0	0	0
F3	0	0	29	1	0	0	0	0	0	0	0	0	0
F5	0	0	1	29	0	0	0	0	0	0	0	0	0
E1	0	0	0	0	30	0	0	0	0	0	0	0	0
E3	0	0	0	0	0	30	1	0	0	0	0	0	0
E5	0	0	0	0	0	0	29	0	0	0	0	0	0
U1	0	0	0	0	0	0	0	22	3	0	0	0	0
U3	0	0	0	0	0	0	0	8	25	0	0	0	0
U4	0	0	0	0	0	0	0	0	2	30	0	0	0
R1	0	0	0	0	0	0	0	0	0	0	30	0	0
R3	0	0	0	0	0	0	0	0	0	0	0	30	0
R4	0	0	0	0	0	0	0	0	0	0	0	0	30

3.7 Discussion

Although there are no studies available in terms of torque classification for performance comparison, the high accuracy of the classifier seems appropriate for torque prediction supporting the idea of recognizing the amount of torque along with the direction by separating the data into different classes. There are many muscles associated with the control of the wrist from which sEMG data can be collected for torque prediction but the number of muscles should be kept as low as possible to form a system with less complexity. The four forearm muscles chosen provided adequate data to recognize the torque of the wrist in different directions.

The confusion matrices in the previous section show that the errors in classification are mostly in the adjacent classes and that these errors reduce with the reduction in the total number of classes. These results also show that the errors in classification is not in the direction of motion but only in the amount of torque applied in a particular direction. This means that the system will not confuse the direction of movement and if the mechanical system is designed keeping in view the errors in torque prediction, the inertia of the system can easily cater for such errors and a smooth output can be observed by the system. The total number of classes in the classification system can be chosen based on the requirements on the smoothness of the output torque and the required accuracy for a particular application.

While the accuracy of the classifier was quite high, it should be noted that there are several factors that were constrained in the experimental setup which

might not be the case in real world applications. Firstly, the wrist of the volunteer was always kept at a neutral position and the performance of the classifier can decrease if the angle of the wrist is changed. This is because the muscles change their position and length depending upon the orientation of the hand which might change the input signals to the classifier decreasing the accuracy. This effect might also be observed during pronation and supination of the forearm. Secondly, there was no actual movement of the wrist due to which there is not much motion artifacts in the input sEMG signals. Thirdly, the amount of torque applied by the wrist was kept at a particular level by the visual feedback on the computer screen. Changes in these levels might also affect the classifier accuracy. Similarly there are numerous physiological factors changing with time which changes the sEMG input to the system such as skin impedance and muscle fatigue. In order to cater such changes an adaptive algorithm can be developed which can train the classifier online and maintain its accuracy.

In summary the proposed technique seems to classify with reliable accuracy when analyzing the data offline with some constraints and provided a basis for further investigation.

CHAPTER 4 EXOSKELETON HARDWARE AND CONTROL

After verification of the classification system, there was a need to test the system on a hard ware in real-time. For this purpose some sort of exoskeleton was needed. Keeping in mind the basic requirements of portability, weight and ease of use, different wrist exoskeleton prototypes (WEP) were developed by the MENRVA research group. Each of these designs used DC motors for movement and the scope of this thesis was to design custom electronics for motor driver as well as algorithms for position and force control for the WEPs and testing their functionality. A generic electronic box was developed along with software algorithms which are explained in detail in this chapter along with the mechanical descriptions of the WEPs.

4.1 Wrist Exoskeleton Prototypes (WEPs)

The first version of the WEP, developed by Henry et al. [52], was a very simple design capable of moving the wrist in just one degree of freedom. The mechanical prototype consists of a rigid arm brace, and a flexible glove, rigidly attached to the hand. A linear actuator (Firgelli L12-50-210-12-P) is mounted on top of the arm brace. The actuator is attached to the glove via cables, routed over cantilevered sections of the brace. Activation of the actuator for the upper forearm exerts a pulling force on the glove, resulting in extension of the hand at the wrist joint while the activation of the lower actuator will result in flexion of the

hand. CAD drawings of the braces prototyped are shown in Figure 4-1. Figure 4-2 shows the two braces with mounted linear actuators as worn by a volunteer.

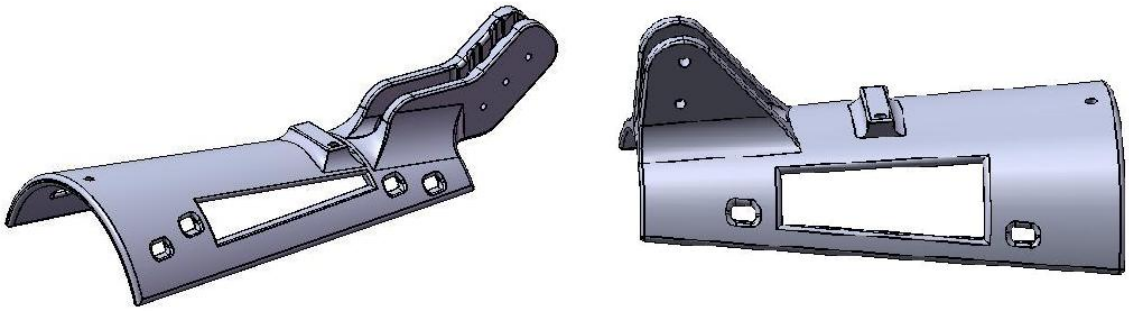

Figure 4-1: CAD drawing of the first WEP [52]

(a) Upper brace, (b) Lower brace

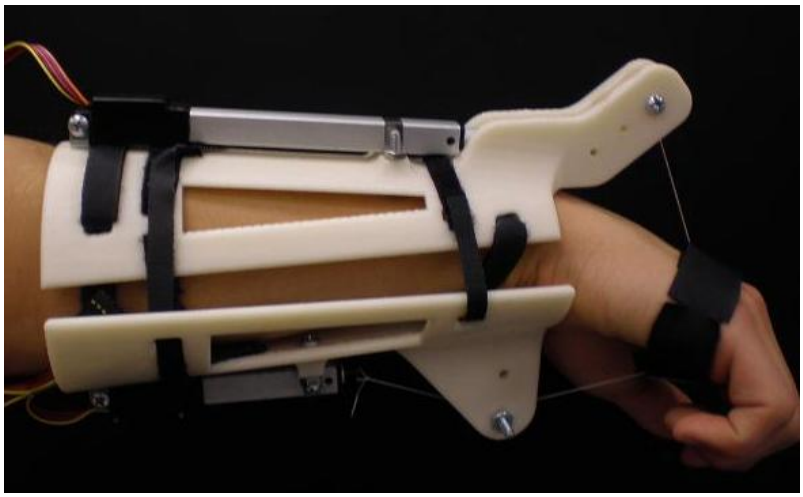

Figure 4-2: Picture of first WEP worn by a volunteer [52]

The second version of the WEP, developed by Khokhar et al. [53], implemented two degrees of freedom. The CAD drawing of the exoskeleton is

shown in Figure 4-3 and Figure 4-4 shows a volunteer wearing the WEP. This prototype mainly consists of a forearm brace, a rigid hand support and two linear actuators (Firgelli L12-100-210-12-P and Firgelli L12-50-210-12-P). Each actuator is mounted on a rotatable base which is connected to the forearm brace by a revolute joint. The forearm brace and the hand support will be secured by using the Velcro straps. When the user wears the exoskeleton, the center of the wrist should be coincident with the intersection of the two axis of the actuator base joint. This will allow the exoskeleton to provide a smooth motion during operation.

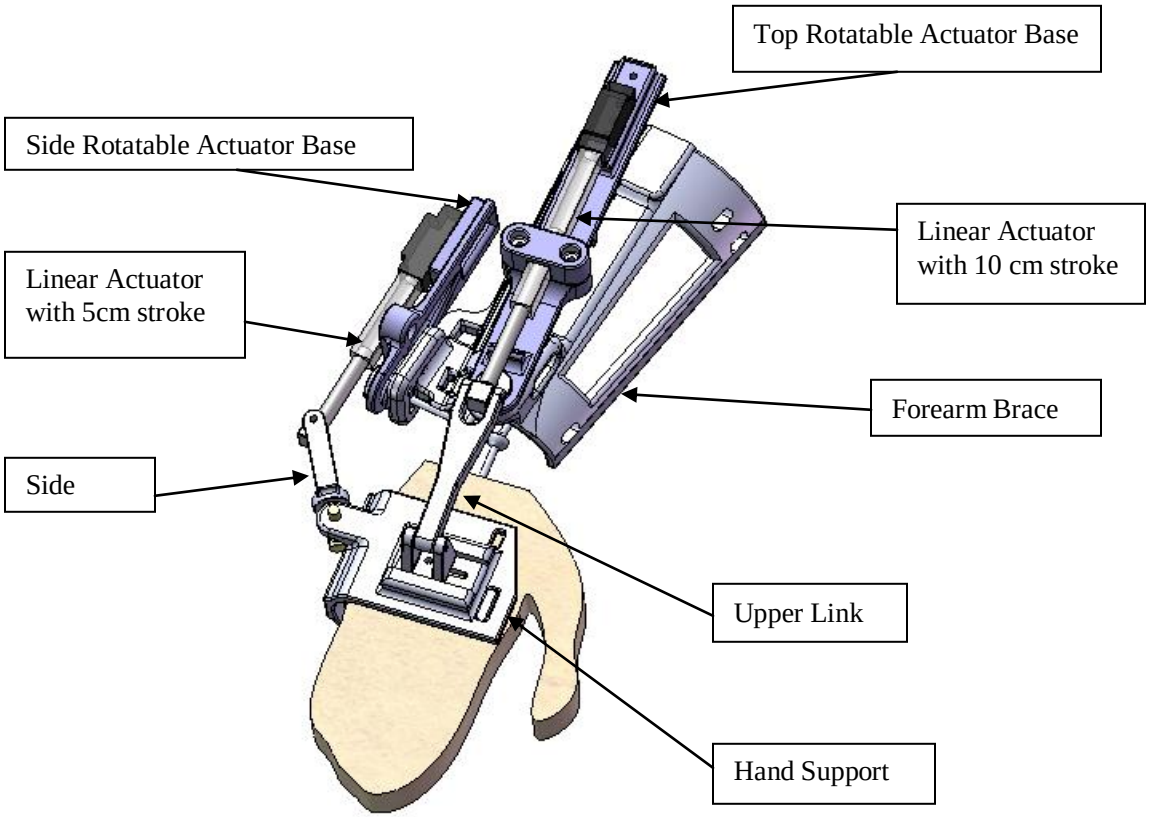

Figure 4-3: CAD drawing of the second WEP [53]

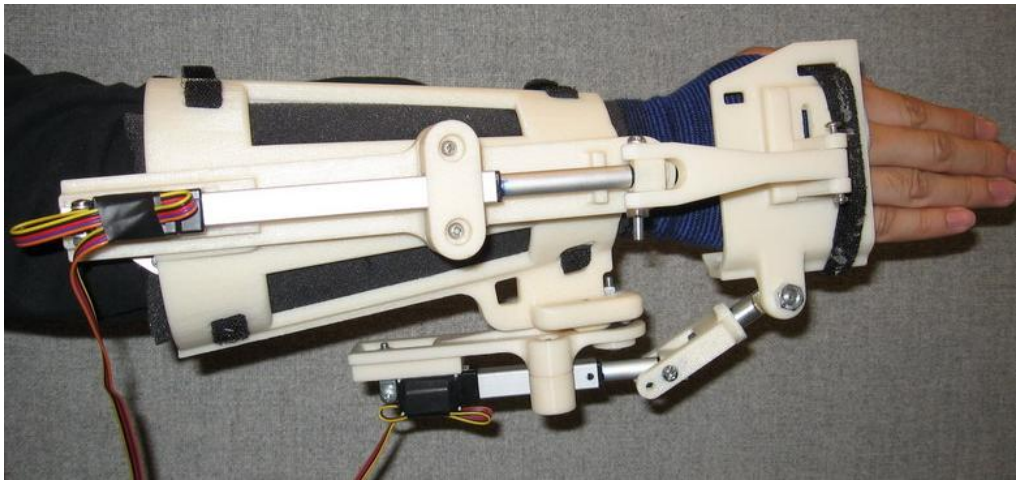

Figure 4-4: Picture of second WEP worn by a volunteer [53]

The third WEP was a modification to the second for better performance. This prototype is made of ABS plastic and mainly consists of two braces for the forearm and the hand. The overall size of the forearm brace is 19.7cm × 16.8cm × 11.1cm and the size of the hand brace is 7.0cm × 12.4cm × 6.0cm. With a total weight of about 500 g including actuators, the WEP is easy to carry and allows the user to potentially wear it in different environments. To prevent possible injures, the WEP motion was mechanically restricted to 60 degree for wrist flexion, 60 degree for extension, 30 degree for radial deviation and 30 degree for ulnar deviation. Further constraints can be applied for different users.

The flexion/extension motion is provided by a linear actuator, having 10 cm stroke length (Firgelli L12-100-210-12-P), which is fixed to a moveable housing coupled to an arc-shaped disk of the forearm brace, as shown in Figure 4-5. The head of the linear actuator is connected to a block having two aluminum square rod extensions used to improve the stiffness during actuation. Two

parallel bars are attached to connect the aluminium extensions with the hand brace through revolute joints. To control the ulnar/radial deviation of the wrist, a gear motor (Pololu 298:1 micro metal gear motor) is attached to a side of the linear actuator housing, and coupled to the outer side of the arc-shape disk with a spur gear. A picture of this WEP is shown in Figure 4-6.

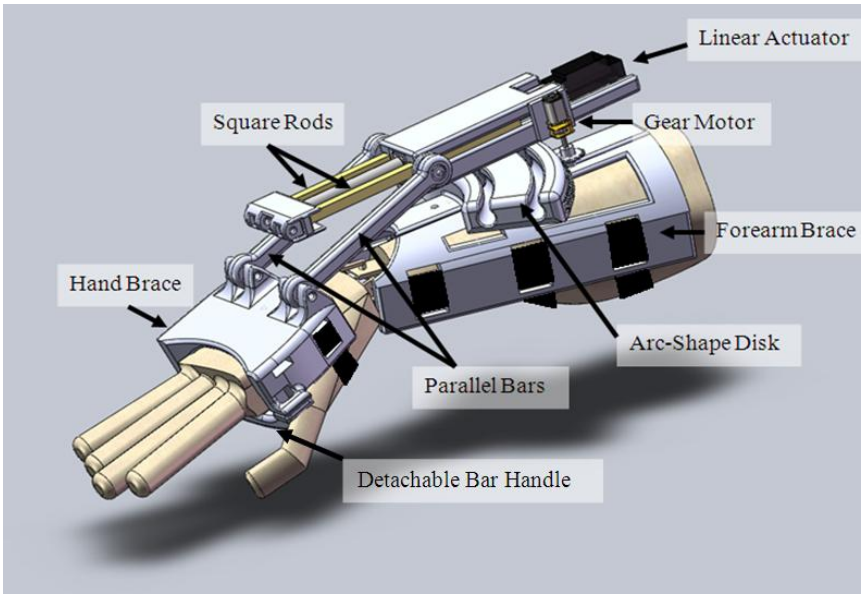

Figure 4-5: CAD drawing of the third WEP

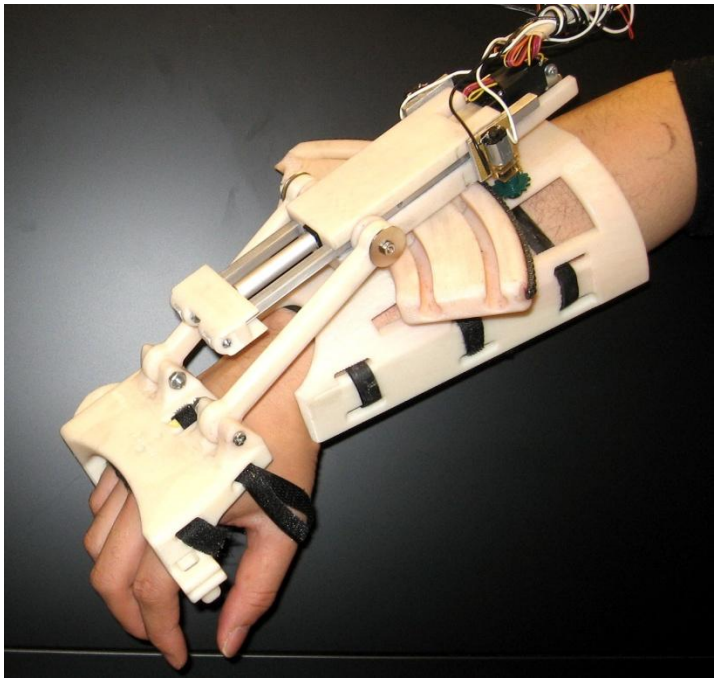

Figure 4-6: Picture of third WEP worn by a volunteer

4.2 Motor Driver Circuitry

All the developed WEPs used DC motor for the movement of the wrist. Therefore, it was important to design the driver circuitry in a way that any dc motor could be controlled using the same electronics. For this reason an electronic box was developed that could be interfaced with a data acquisition board (DAQ). The details for this electronic box are described in the following sections:

4.2.1 Hardware

The Hardware for the driver mainly consists of an L298 Full bridge driver IC. A PWM signal is used to control the DC voltage to the motor connected with

the driver IC. For our application we needed to control two linear actuators at a time which requires 4 PWM signals for full bridge operation. However we only had 2 frequency outputs in our DAQ that could generate the required PWM signal at a frequency of 20 KHz. To overcome this issue we used a 74HC08 quad 2 input AND gate IC which allowed us to control each motor by using just one PWM signal. There where sense resistors on the sense output of the L298 used to measure the amount of current flowing through the motor. The voltage signal across the sense resistors are amplified by using an instrumentation amplifier INA122P followed by a low pass filter at around 48 Hz. This feedback provided us with a reasonable approximation of the force applied by the actuator. Our linear actuators also provided potentiometer feedback for the position but these were distorted due to the PWM operation. Therefore we passed the feedback through a low pass filter at 48 Hz before inputting it to the DAQ card.

4.2.2 Schematic

The schematic Diagram for the circuit is provided in Figure 4-7. This schematic was generated using Eagle SoftCAD.

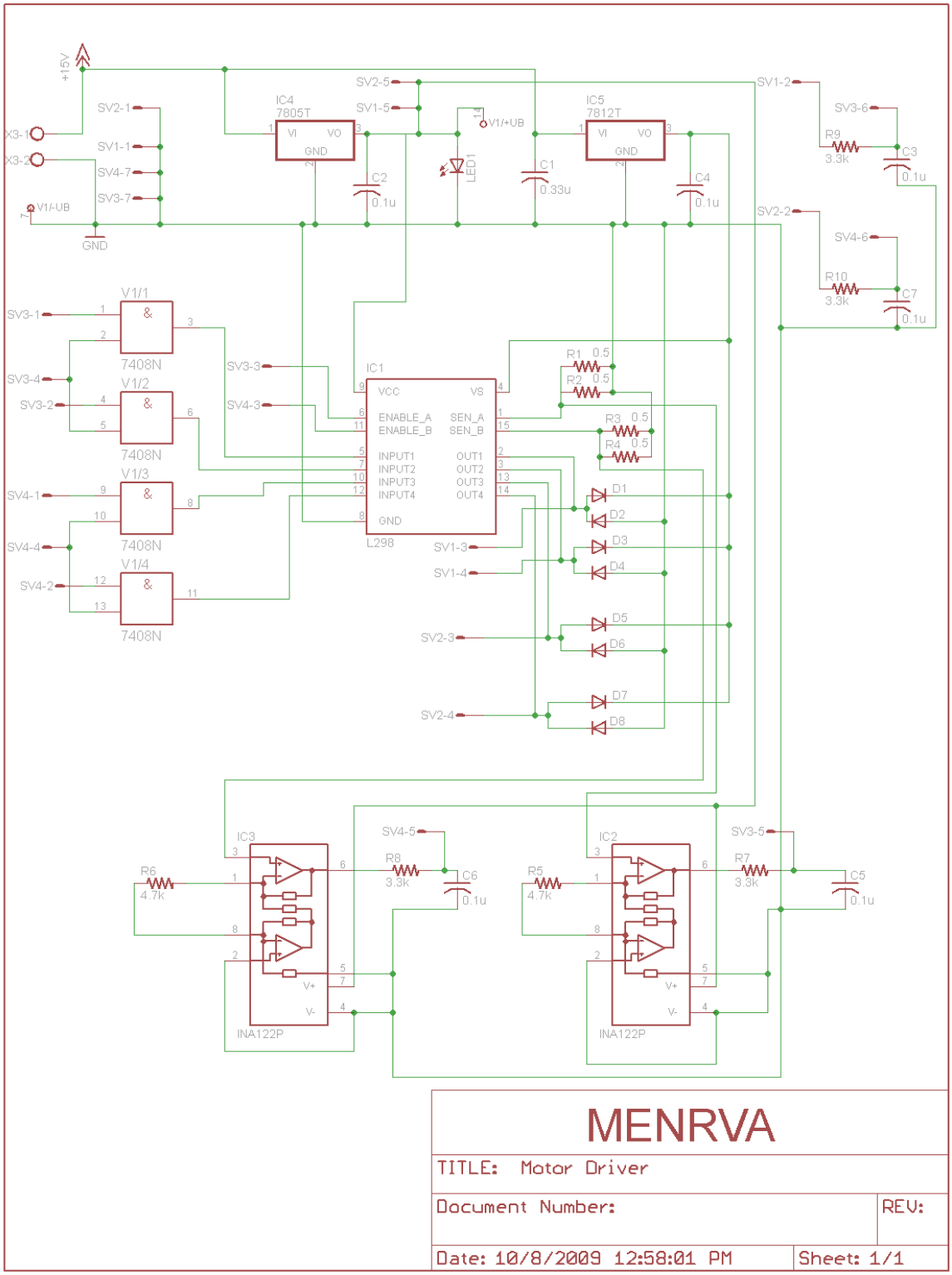

Figure 4-7: Schematic of the electronic circuitry

4.2.3 Electronic Board

The electronics board was fabricated on a PCB. There are currently two boards fabricated, one using a single layer PCB and the other using a double layer PCB. The operation of both is similar. The layout of the components on the board is shown in Figure 4-8.

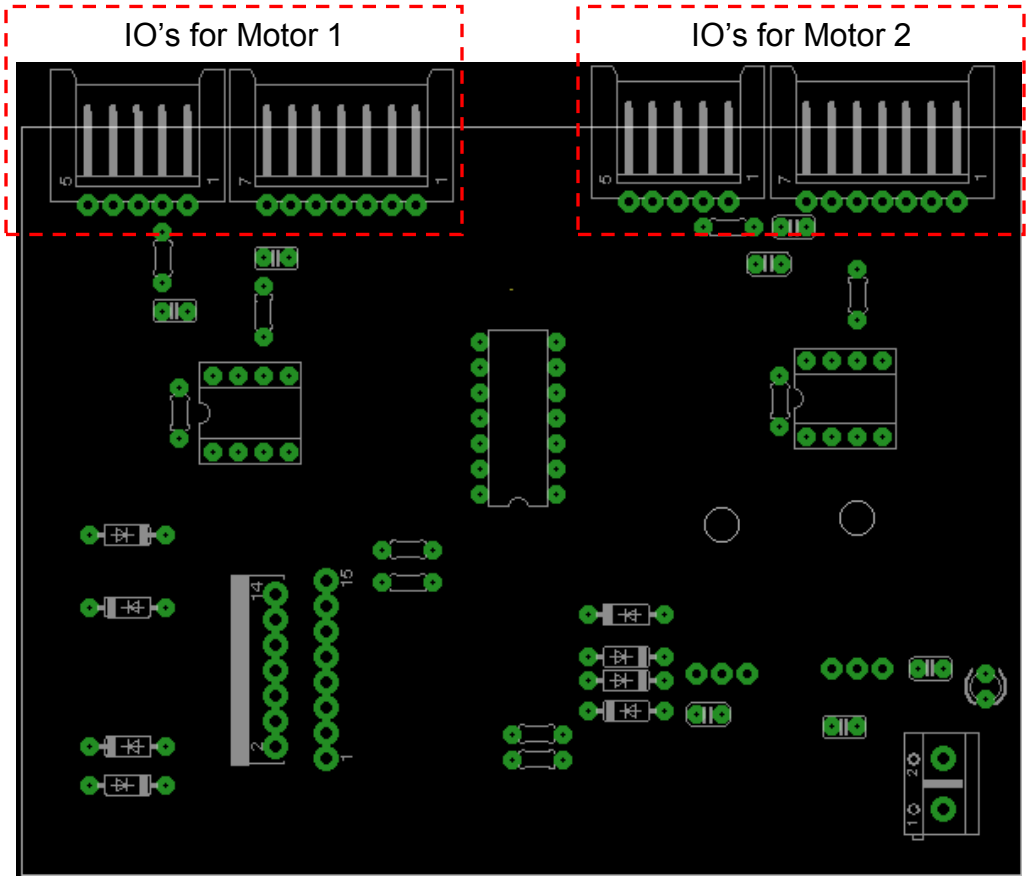

Figure 4-8: PCB board layout for the electronic circuitry

4.2.4 Pin Outs for Electronic Circuitry

Externally the board can be connected with dc motors and any controller or DAQ card by the MTA-100 series connectors. There are 4 connectors

available on the board (SV-1, SV-2, SV-3 & SV-4). SV-1 & SV-3 forms a pair to control one motor and SV-2 & SV-4 forms the pair to control another motor separately. The pairs are identical. The motor connectors SV-1 & SV-2 configuration is given in Table 4-1 and the control connectors SV-3 & SV-4 configuration is given by Table 4-2. The type specified in the tables corresponds to the device's perspective, e.g. in SV-1 motor is the device, so an input means input to the motor. Similarly in SV-3, the controller or the DAQ is the device, so input means input to the controller or DAQ.

Table 4-1: Pin configuration for motor connectors SV-1 & SV-2

Pin Number	Function	Type
1	Potentiometer excitation -	Input
2	Position feedback from potentiometer	Output
3	Motor excitation +	Input
4	Motor excitation -	Input
5	Potentiometer excitation +	Input

Table 4-2: Pin Configuration for control connectors SV-3 & SV-4

Pin Number	Function	Type
1	Direction pin 1	Output
2	Direction pin 2	Output
3	Enable	Output
4	PWM signal	Output
5	Current Input	Input
6	Position Input	Input
7	Gnd	-

4.2.5 Timing Diagram for Control Inputs

A timing diagram is shown in Figure 4-9. When the actuator is extending or retracting, the speed is controlled by the PWM signal (not shown in diagram).

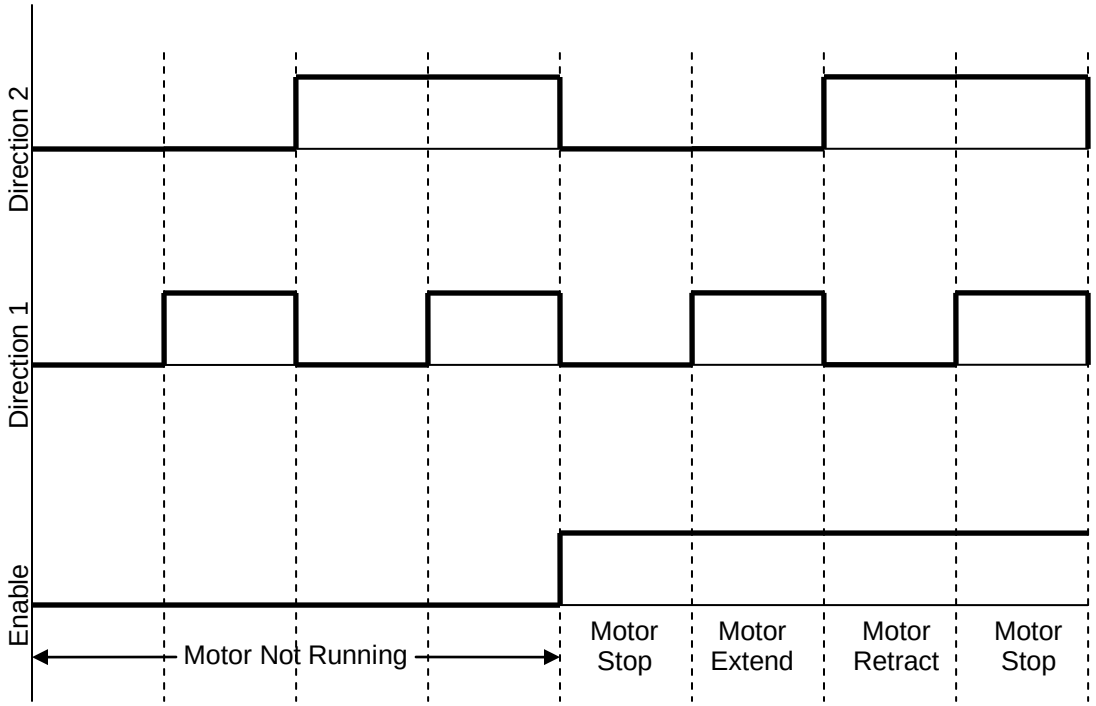

Figure 4-9: Timing diagram for motor control signals

4.3 Position Controller

The linear actuators used in the WEPs provided a simple position feedback through a potentiometer. This feedback was used to control the extension/retraction of the rod of the actuator. The desired set point from the user or the software was compared to the potentiometer feedback and depending upon the difference, the direction of movement is decided. A small tolerance (tol) was introduced to cater for the precision of the potentiometer feedback. The implementation philosophy is shown in Figure 4-10.

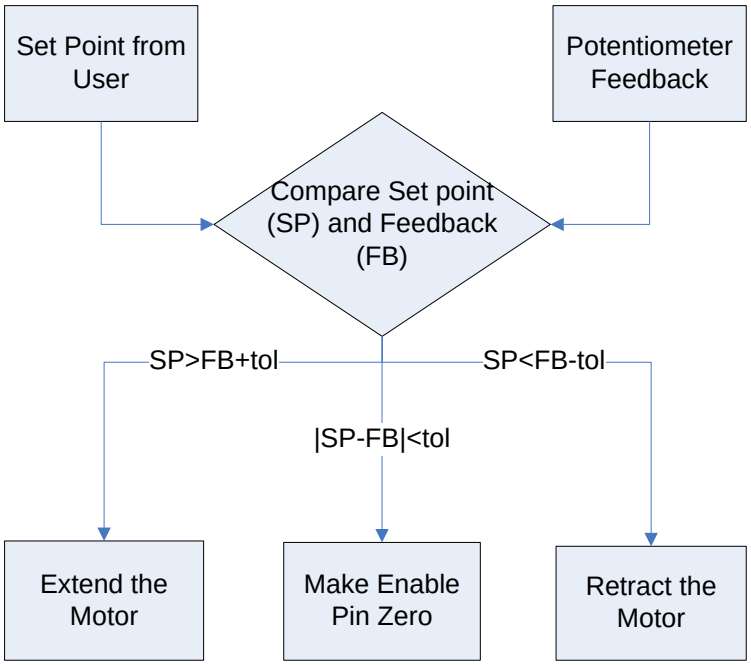

Figure 4-10: Position control philosophy

The position control philosophy was implemented using LabVIEW software and then tested at different set points from the user. A vernier calliper was used to measure the actual extension of the rod. Both types of linear actuators with 100m stroke length and 50 mm stroke length were tested during extraction and retraction. The results of the testing are presented in Table 4-3.

Table 4-3: Results for position control testing

100 mm Stroke Length			50 mm Stroke Length		
SP (mm)	Extending (mm)	Retracting (mm)	SP (mm)	Extending (mm)	Retracting (mm)
0	0.76	1.06	0	1.06	1.1
10	10.62	9.66	10	12.62	14.5
20	20.46	19.02	20	24.2	24.96
30	29	29.64	30	33.1	35.28
40	40.36	41.06	40	43.54	44.28
50	51.06	51.84	50	51.1	51.1
60	62.98	63.28			
70	73.6	74.58			
80	84.66	84.9			
90	93.14	93.82			

4.4 Force Controller

For a dc motor such as the one used by the linear actuator, there is a linear relationship between the force applied by the motor and the current flowing through it. If very precise force control is not needed, as in our case, it is a good idea to control the current flowing through the motor rather than the use of expensive sensors. This current control was used as the basis for the force control philosophy in the implementation. As there was a driver circuitry along with amplifiers for current feedback, obtaining the relationship between force and current through the actuator's datasheet was not accurate and an experimental approach was utilized. Using the same electronic hardware as described before, different data points were obtained to draw a graph between the current flowing through the actuator and the force applied by it. The force applied was measured by a force sensor (Futek LCM 300). The obtained graph is shown in Figure 4-11 and the established relationship is given by equation 3-1.

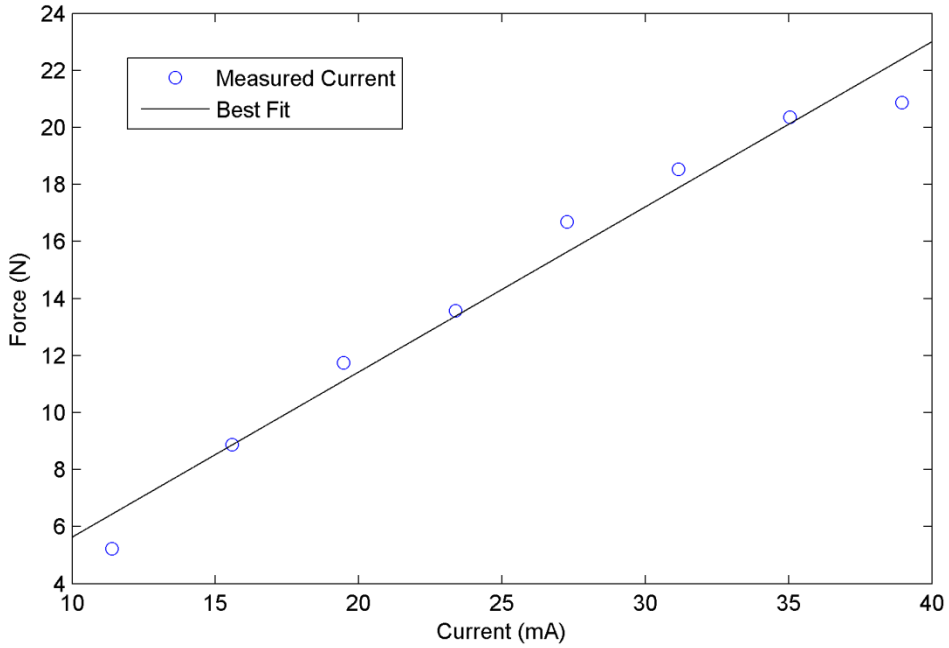

Figure 4-11: Relationship between input current and output force by the linear actuator

$$F = 0.5791I - 0.1575 \quad (3\text{-}1)$$

Where *F* is the force applied by the actuator when current *I* is flowing through it. After making the desired force set point compatible with the feedback, a variable X initialized to zero is compared to the set point. If the set point is greater than X by a predefined tolerance (tol) then the actuator is supplied with full voltage corresponding to a 100% duty cycle to the pulse width modulated (PWM) signal and value of X is updated to the current feedback. This ensures that the actuator operates at its maximum speed. If X becomes greater than the set point by the predefined tolerance (tol) then X is fixed to the current value and the PWM signal is controlled by the output of a PID controller. The value of X is updated to the value of the current feedback once the current reaches the

desired set point. This strategy insures that the force exerted by the actuator does not exceed the desired set point. The force control philosophy is represented graphically in Figure 4-12.

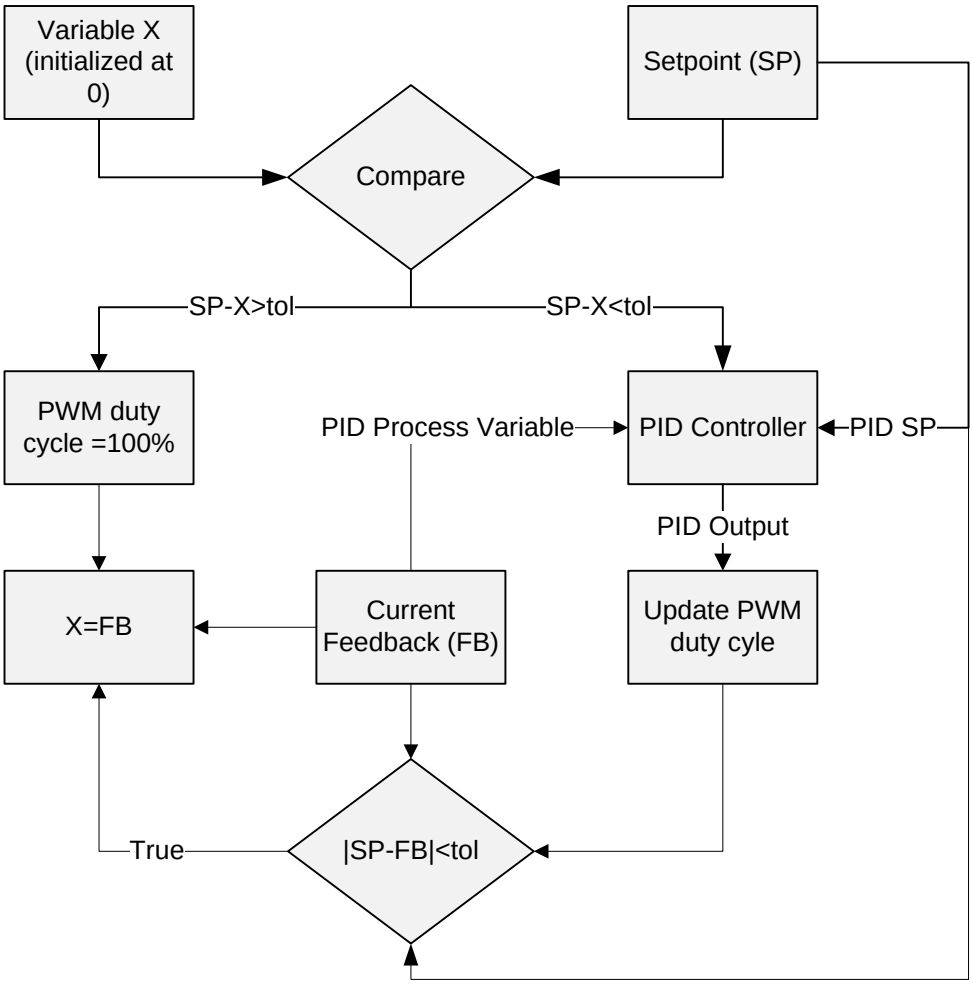

Figure 4-12: Force control philosophy

This force control philosophy was implemented using LabVIEW application. Different set point were given to the application and the force produced by the actuator was recorded using a force sensor. The experiment

was repeated five times at each set point. The results obtained for the force control are presented in Table 4-4.

Table 4-4: Results for force control testing

Set Point (N)	Mean of Obtained force	Standard Deviation of obtained force
10	8.654	0.641896
15	15.442	0.284816
20	17.844	0.435063

4.5 Discussion

Having generic position and force control strategies provides a great freedom in developing different applications for the mechanical exoskeletons and testing the performance of new designs. By using these modules as building blocks, an application for a rehabilitative system was developed using one of the exoskeletons, details of which can be found in Appendix B. This device is being used in an experimental procedure for rehabilitation of stroke patients. The developed force control strategy is also utilized in developing an assistive device, for which proof of concept is presented in Chapter 6. In summary, developing generic electronics and control strategies provided us the freedom to efficiently test new designs and applications which is an important step in achieving the final goal of developing a generic assistive/rehabilitative device.

CHAPTER 5 REAL-TIME CLASSIFICATION SYSTEM

In Chapter 3, a successful classification technique was presented that could identify the intention of the user in terms of force and direction. Chapter 4 presented the developed hardware that could be used for assistive or rehabilitative purposes. But in order to use the proposed classification technique on the hardware, there was a need to develop an application that could perform classification in real-time. For this purpose the LabVIEW platform was chosen for application development. This Chapter describes the implementation of the application, the experimental setup used and the results obtained for the real-time classification system.

5.1 Application Development

There are two main components of an application developed in LabVIEW namely the front panel and the back panel. The front panel is a graphical user interface which is used for input/output to an application. The back panel implements the algorithm for the application in its own graphical programming language. Both these components are explained in detail in the following sections.

5.1.1 Front Panel

The front panel for the application is shown in Figure 5-1. This is the interface used to gather the training data for a volunteer and switch between the two modes of operation; data gathering and prediction. The left most part of the front panel consists of two bar graphs. One of these bar graphs shows the normalized torque applied by the wrist of the volunteer in real-time. This is important to apply a torque corresponding to a particular class and recording appropriate data for training the classifier. The second bar graph shows the force applied by the exoskeleton as will be explained in the experimental setup section. Above the bar graphs is the output of the classifier which works when the application is in the prediction mode.

The user starts in the data gathering mode. The numeric control labeled “class” specifies for which class the data is being recorded. The user should select this class based on the torque applied by the user indicated by the bar graph. The variable “class_x_index” (x is class number) indicates the number of samples collected for a particular class. When the required number of samples are acquired the “t_data_cx” light indicator turns on and the training data can be seen in the variable “class_x_train”. In this fashion all the training data for 13 classes is acquired. The user then presses the train button which trains the classifier and then shows the parameters of the SVM in the “output cluster” along with cross validation accuracy. The user can then change the mode of the application to prediction which then predicts the class based on the torque applied by the volunteer.

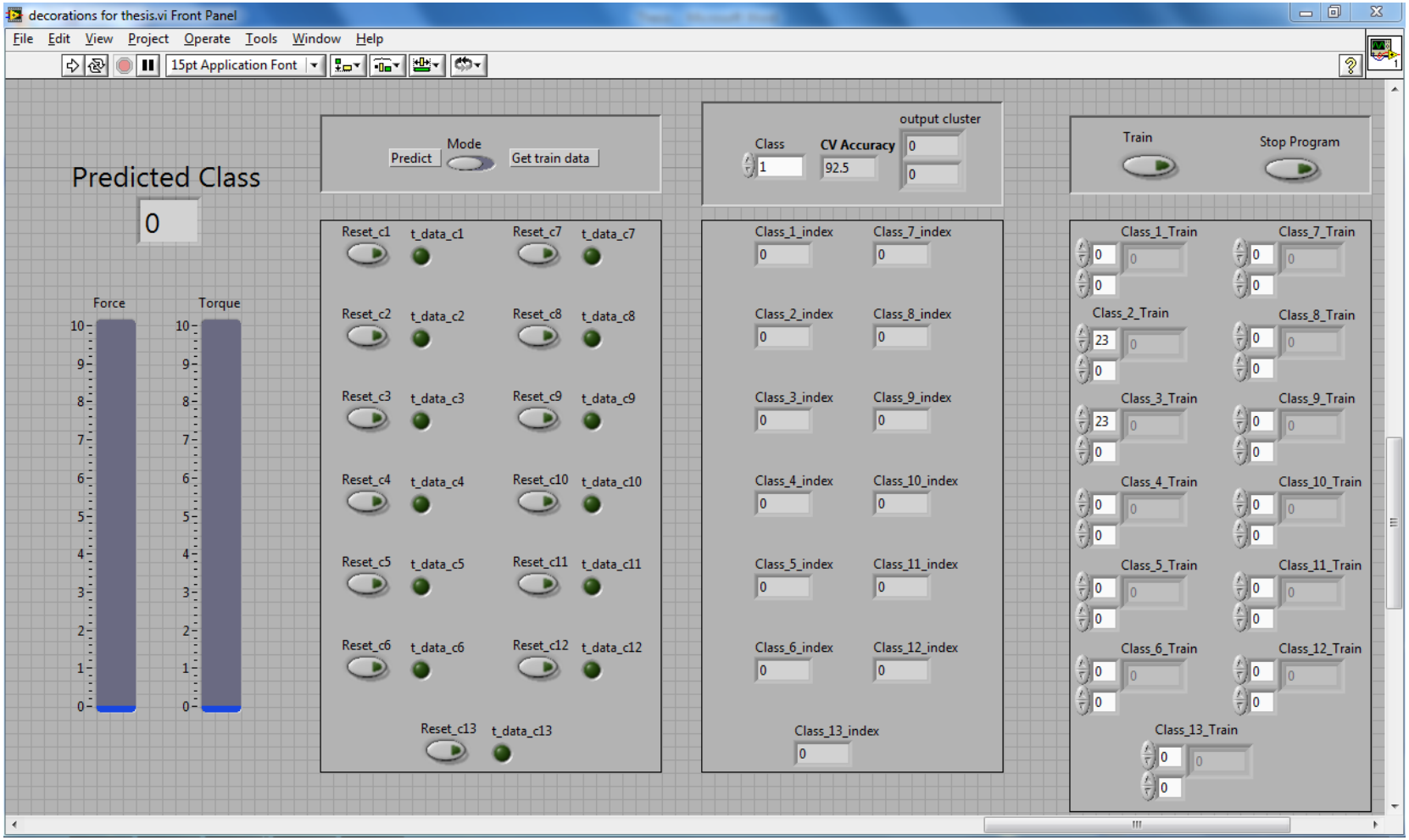

Figure 5-1: Front panel for real-time classification application

5.1.2 Back Panel

The back panel contains all the programming to perform the tasks seen on the front panel. The logical flow of the application is shown in Figure 5-2 and its full implementation is shown in Figure 5-3. The details of the implementation are explained in the following sections.

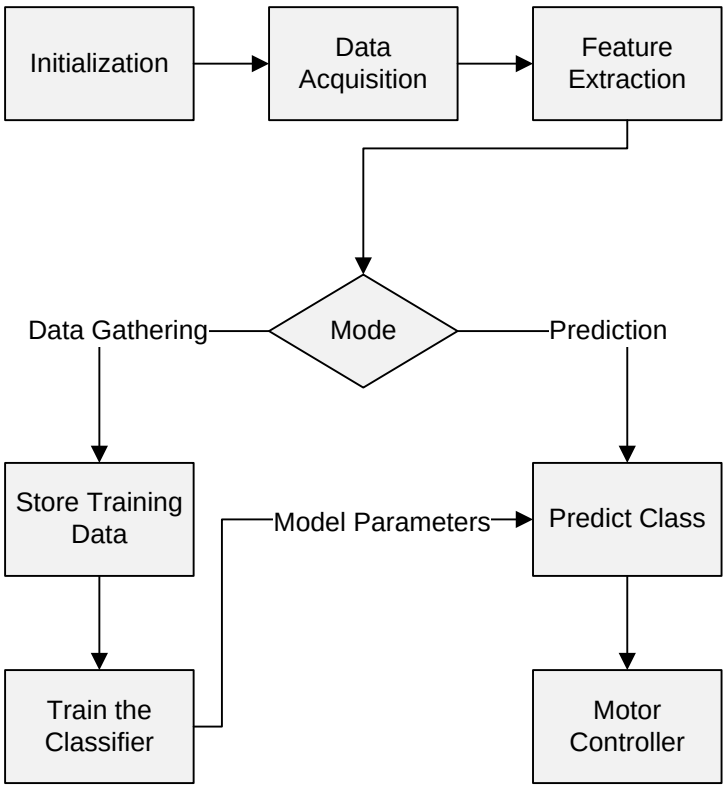

Figure 5-2: Logical flow of real-time classification application

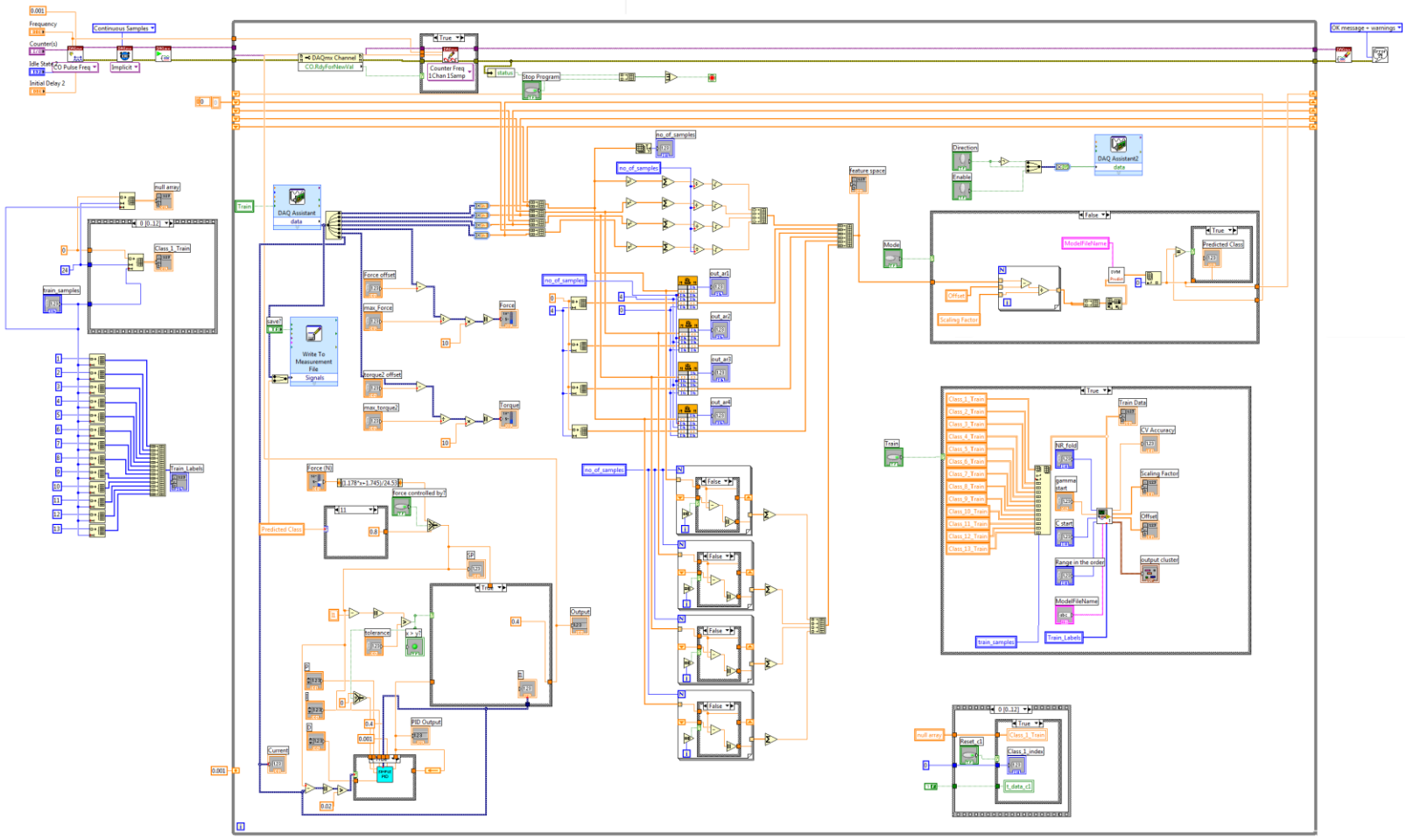

Figure 5-3: Back panel for real-time classification application

5.1.2.1 Initialization

On initialization there is a need to define variables of appropriate size that would hold the data for the training and also initialize the target label vector to be used during training. Figure 5-4 represents the initialization step.

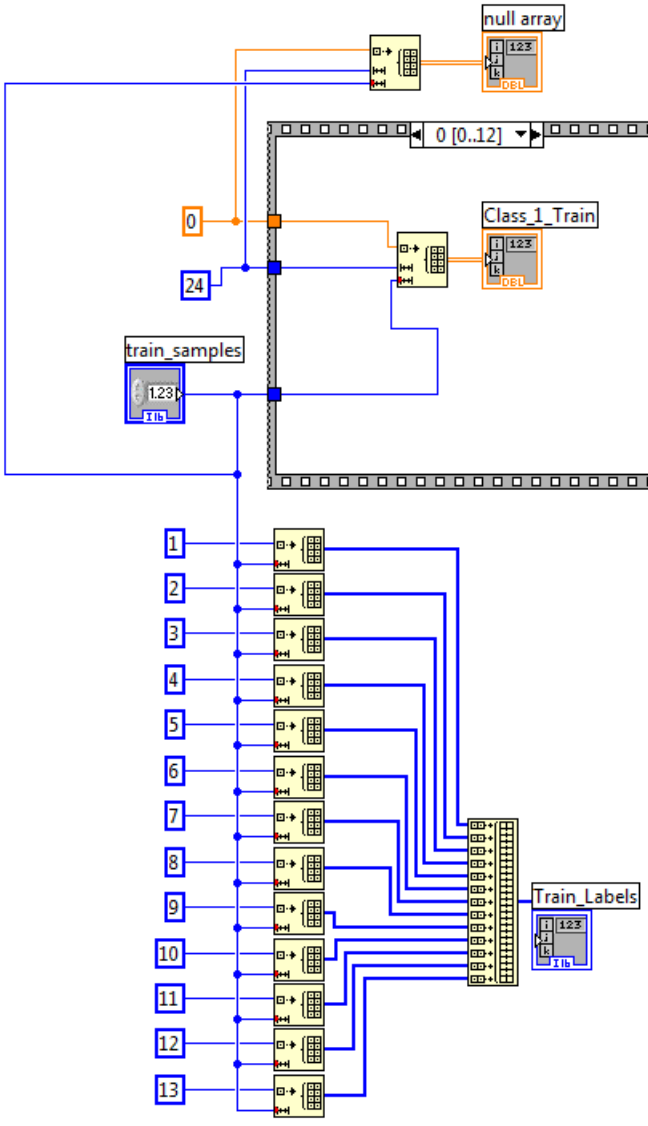

Figure 5-4: Initialization step in application development

A control variable “train_samples” defines the number of samples to be used for the training data. A stacked sequence is used to create 13 array variables of size t x 24 (t is the number defined by variable “train_samples”); one for each class. All the elements in the arrays are initialized to zero. A variable “null array” is also defined to reset any variable for reacquiring the data. An array “Train_Labels” is created which serves as a class label for the acquired training data.

5.1.2.2 Data acquisition and feature extraction

The data from a data acquisition card is introduced into the application by the use of DAQ assistant. The acquired sEMG data from each channel has to be converted into features. As described in chapter 3, three types of features namely rms values, AR model coefficients and waveform length were used. The implementation of converting input sEMG signals to features is shown in Figure 5-5. The implementation for AR model coefficients is done by using a C code block in LabVIEW as there was no predefined block available in the LabVIEW software. Note that the implementation shown is only for a single channel. The application implements the same strategy for each channel of acquired sEMG data. After converting each channel into features, all of the data is converted to a single array of size 1 x 24 (four sEMG channels), which is named “feature space” in the application.

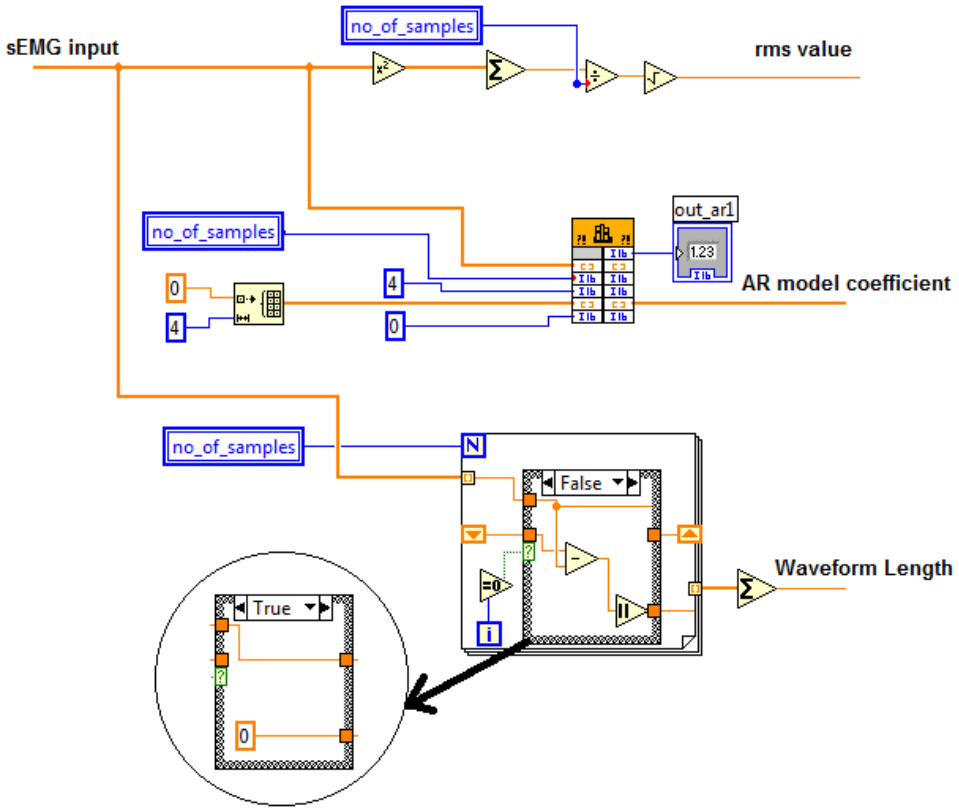

Figure 5-5: Implementation of feature extraction

5.1.2.3 Store Training Data

After extracting the features from the sEMG channels the data had to be stored into variables according to their class labels. The implementation is shown in Figure 5-6. If the number of stored samples is less than the required samples for training then the feature vector is stored in the variable based on the selected class. A stacked sequence is used to store data for each class.

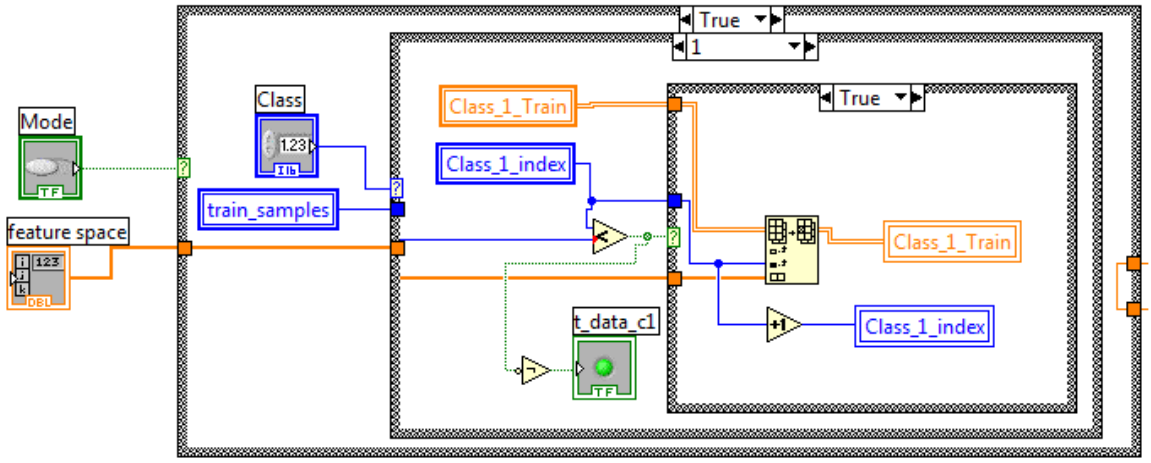

Figure 5-6: Implementation for storing data

5.1.2.4 Training the classifier

The classifier is trained when the user pushes the “train” button on the front panel. LibSVM provides a block of SVM train in the LabVIEW environment that is used in the implementation shown in Figure 5-7. The block shown in the figure for training has been modified to use the best parameters after cross validation. The parameters to be used during cross validation is provided by the user. The data acquired in the variables for storing training data for each class is combined to from the full training data and the labels that were created in the initialization step is used.

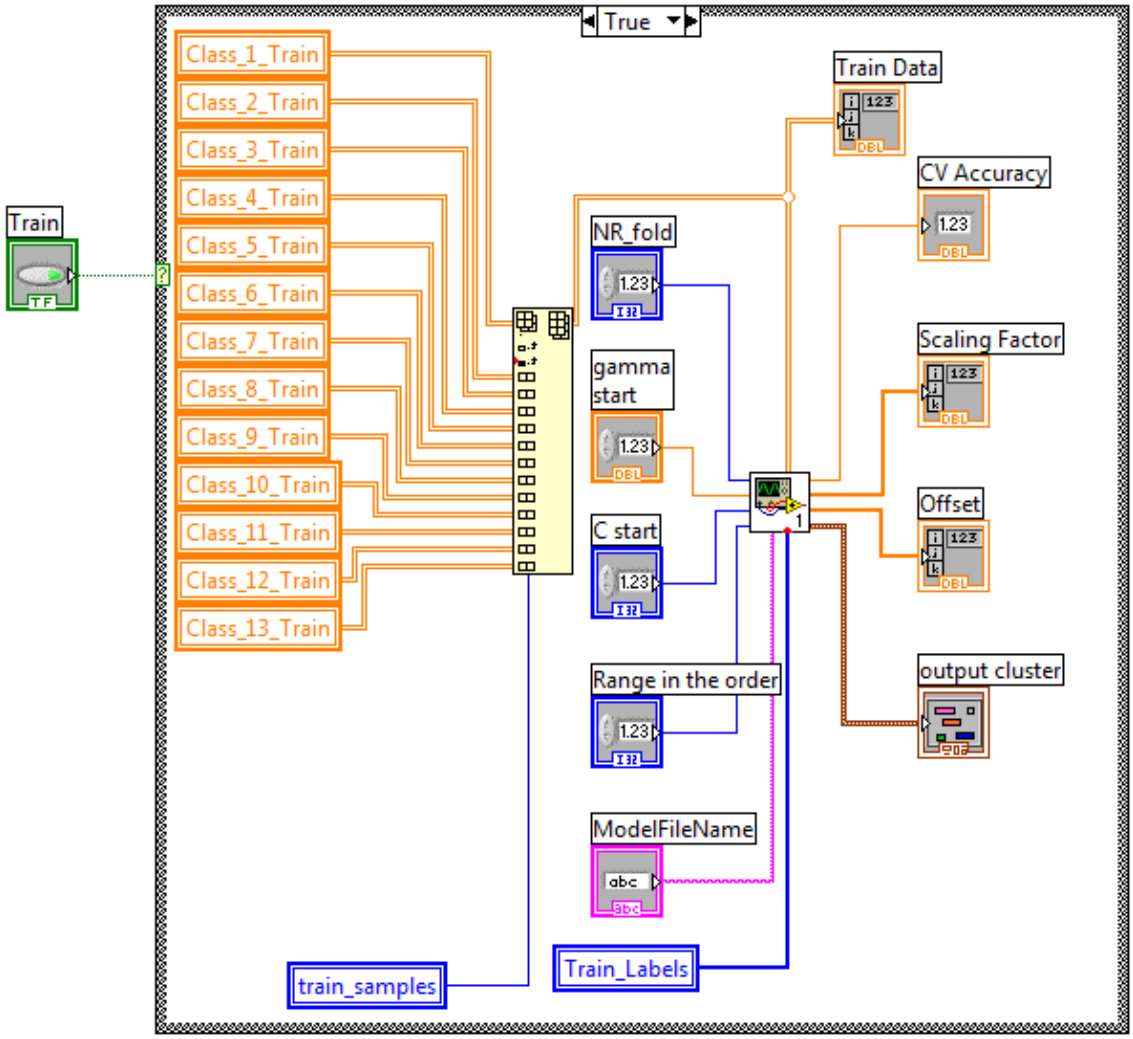

Figure 5-7: Implementation for training the classifier

5.1.2.5 Class Prediction

When the user selects the predict mode, the features from the sEMG channels are no longer stored but fed to the prediction module provided by the LibSVM after scaling and normalization. The SVM model created during training

is utilized and the predicted class is displayed on the front panel and also used for motor control. The implementation is shown in Figure 5-8.

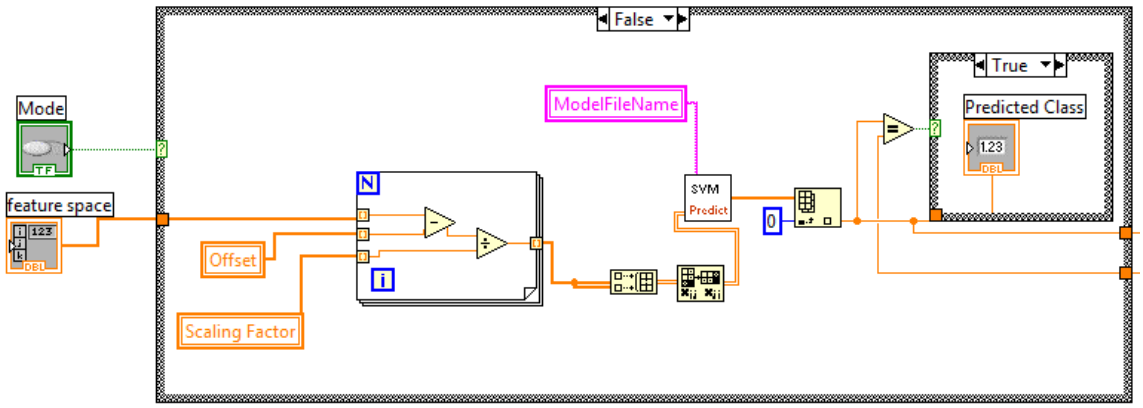

Figure 5-8: Implementation for prediction by classifier

5.1.2.6 Motor Control

After predicting the class, configurable command are provided to the motor controller which can then move the motor. The motor controller uses the same philosophy as described in Section 3.5. Its implementation in LabVIEW is shown in Figure 5-9.

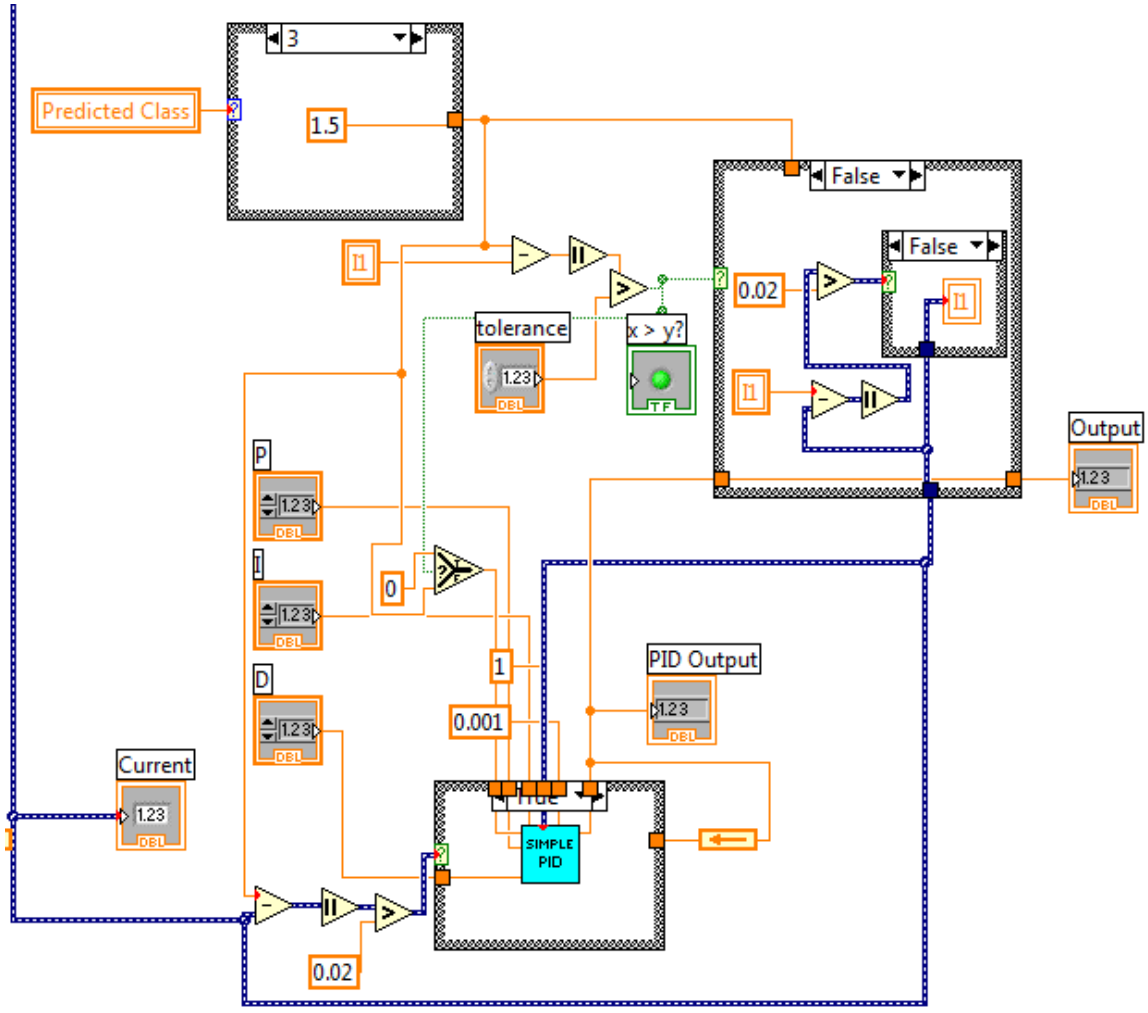

Figure 5-9: Implementation of motor control

5.2 Experimental Setup

To test the performance of the system in real-time, an experiment with the developed LabVIEW application was conducted. A picture of the experimental setup is shown in Figure 5-10. The setup included the custom rigs for measuring the torque produced by the wrist of the volunteer during flexion/extension and ulnar/radial deviation, sEMG acquisition system (Noraxon Myosystem 1400L),

data acquisition card (National Instruments USB-6289), laptop running the LabVIEW application, WEP secured on a wooden palm attached to a platform and a force sensor (Futek LCM300) connected to the wooden palm to record the force produced by the WEP. A block diagram representing the interconnection between the different components is shown in Figure 5-11.

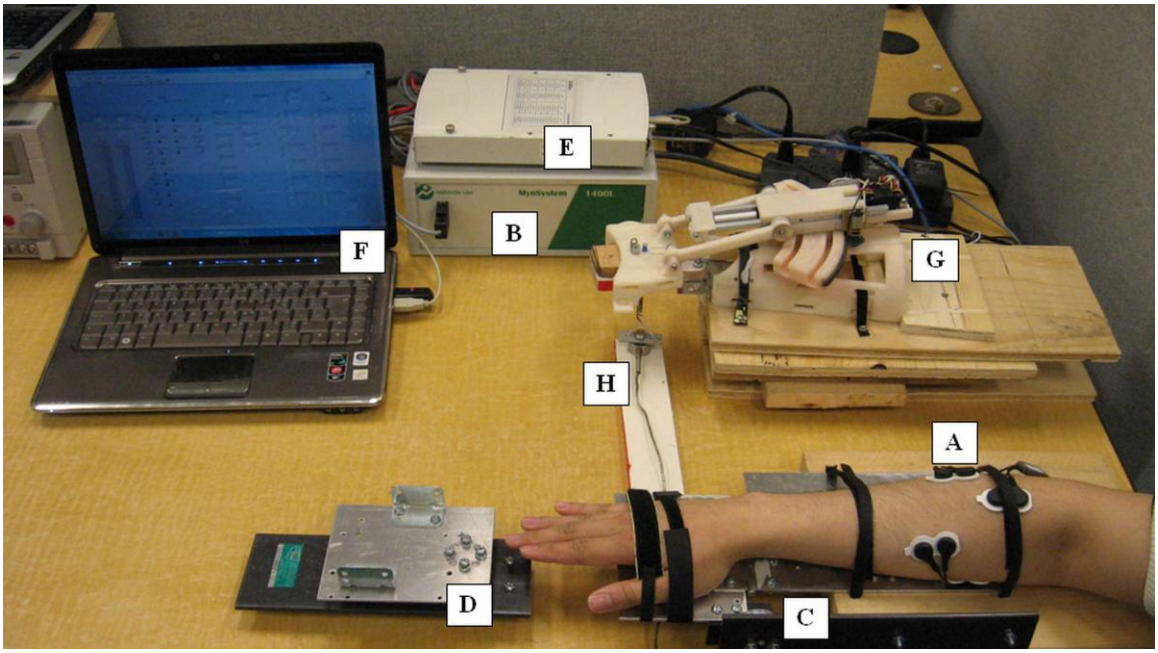

Figure 5-10: Real-time experimental setup

(A) sEMG leads, (B) sEMG measuring device, (C) torque measuring device for wrist flexion-extension, (D) torque measuring device for wrist ulnar-radial deviation, (E) data acquisition board, (F) classifier and force controller in LabVIEW, (G) WEP, and (H) force sensor.

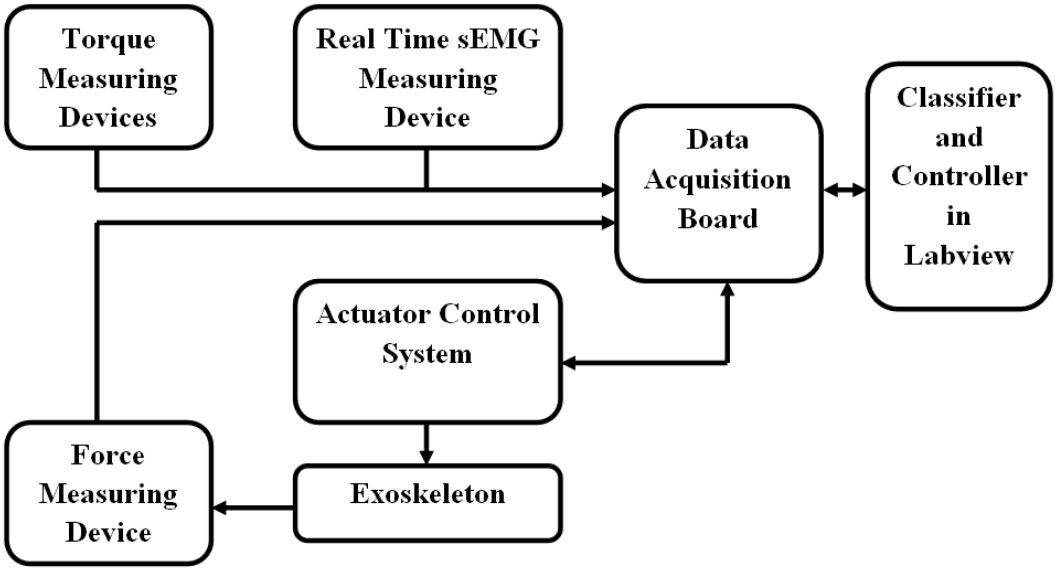

Figure 5-11: Block diagram for real-time experimental setup

The real-time experiment consisted of two steps: training and testing. During the first step, the volunteer was asked to place the right forearm on the custom made rig, which indicated the torque applied by the user in real-time. The sEMG acquisition system, presented in the section 3.1, was used. The torque and EMG data were digitalized at a frequency of 1 KHz. The volunteer applied the torque according to the proposed protocol (see Table 3-1) and 13 classes were trained. In the second step, the volunteer applied different torques by using the same setup and the LabVIEW application predicted the wrist output through the sEMG input and provided the control signal in real time to actuate the WEP, which applied torque corresponding to the identified class.

5.3 Results and Discussion

The performance of the classification system in real-time was studied by controlling the WEP by the sEMG signals of the forearm. A control signal was generated by the system after every 125 ms and the sEMG signals from the data acquisition card was acquired every 125 ms ensuring that the total response time for the system was less than 250 ms. These delays are acceptable for real-time systems as indicated in [45, 46].

Figure 5-12(a) shows the torque applied while the volunteer was flexing the wrist during the testing step of the experiment. The sEMG signals of the muscles, which act as the inputs to the real-time classification system, are shown in Figure 5-12(b-e). It can be observed that the flexor muscle (FCU) is mainly active during this flexion action. The real-time system predicts the intention of the volunteer and the output of the classifier is shown in Figure 5-12(f). Based on the output of the classifier, the system sends control signals to the WEP which responds by applying a force on the sensor. The output of this sensor is shown in Figure 5-12(g). It can be observed that the output force recorded by the sensor (Figure 5-12(g)) directly corresponds to the applied torque by the wrist of the volunteer (Figure 5-12(a)). The results for wrist extension, radial deviation and ulnar deviation are respectively presented in Figures 5-13, 5-14 and 5-15.

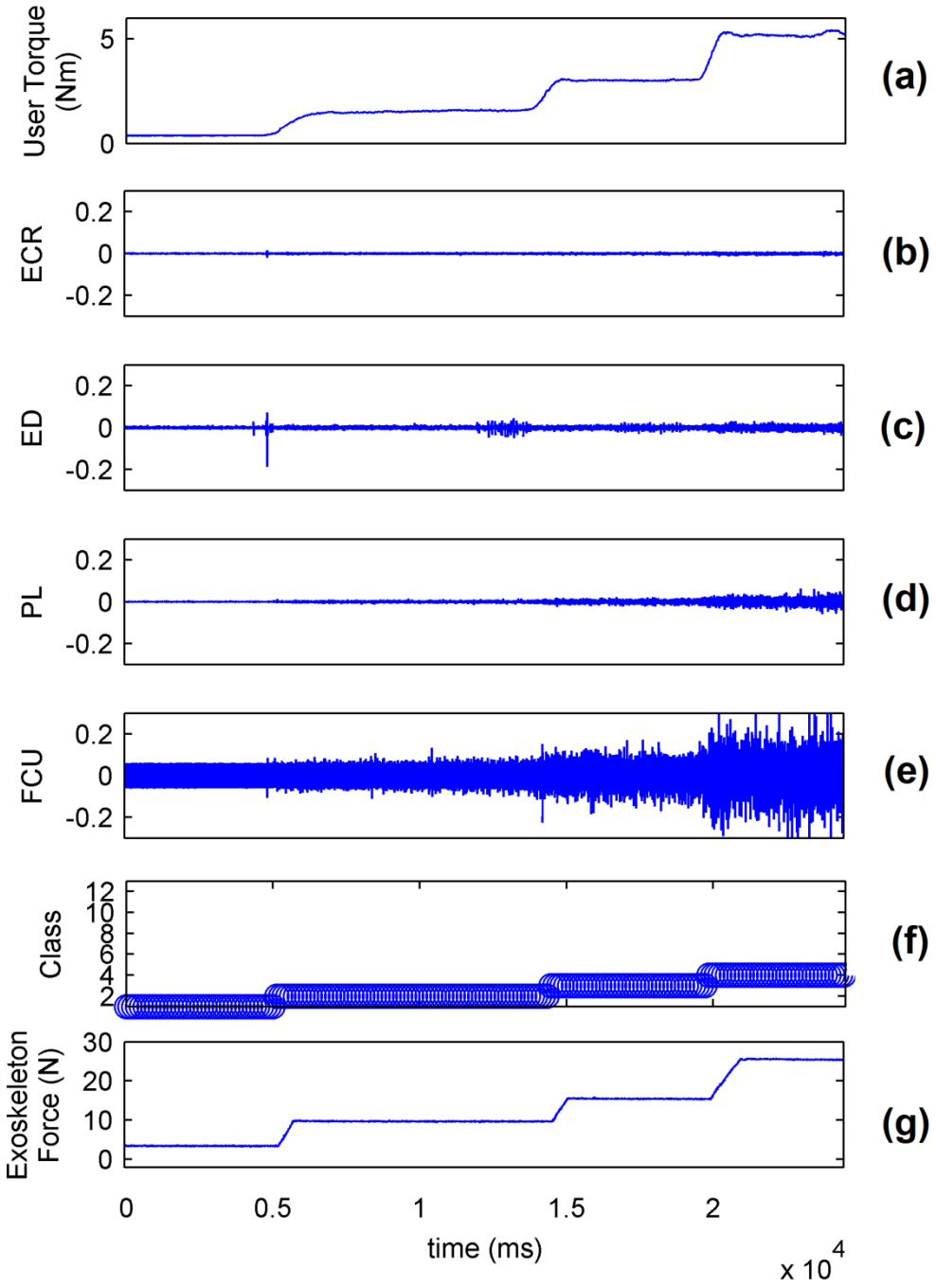

Figure 5-12: System performance for wrist flexion

(a) Torque applied by the wrist of volunteer; (b) ECR muscle activation; (c) ED muscle activation; (d) PL muscle activation; (e) FCU muscle activation; (f) Identified class by the system; and (g) Force applied by exoskeleton.

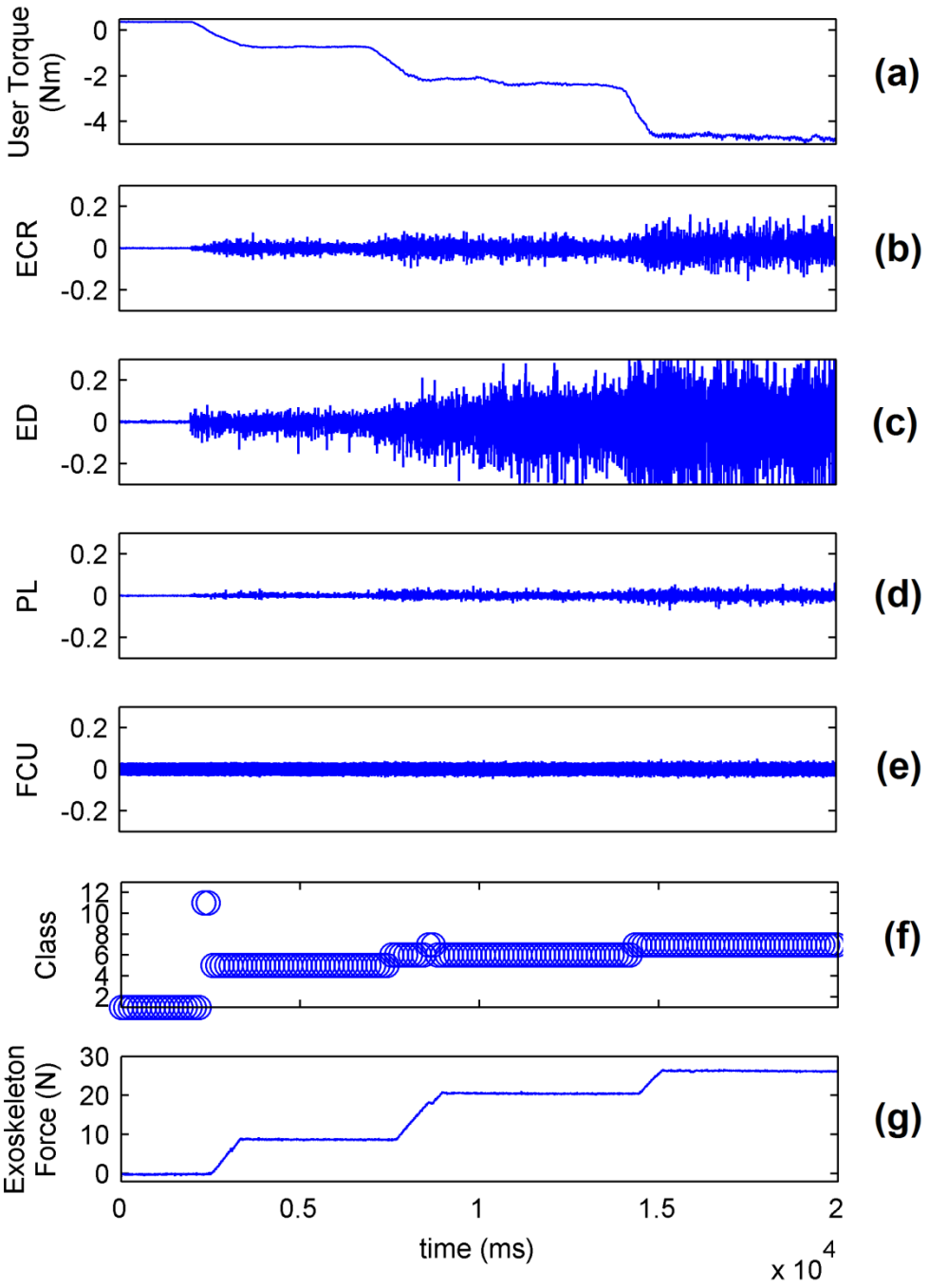

Figure 5-13: System performance for wrist extension

(a) Torque applied by the wrist of volunteer; (b) ECR muscle activation; (c) ED muscle activation; (d) PL muscle activation; (e) FCU muscle activation; (f) Identified class by the system; and (g) Force applied by exoskeleton.

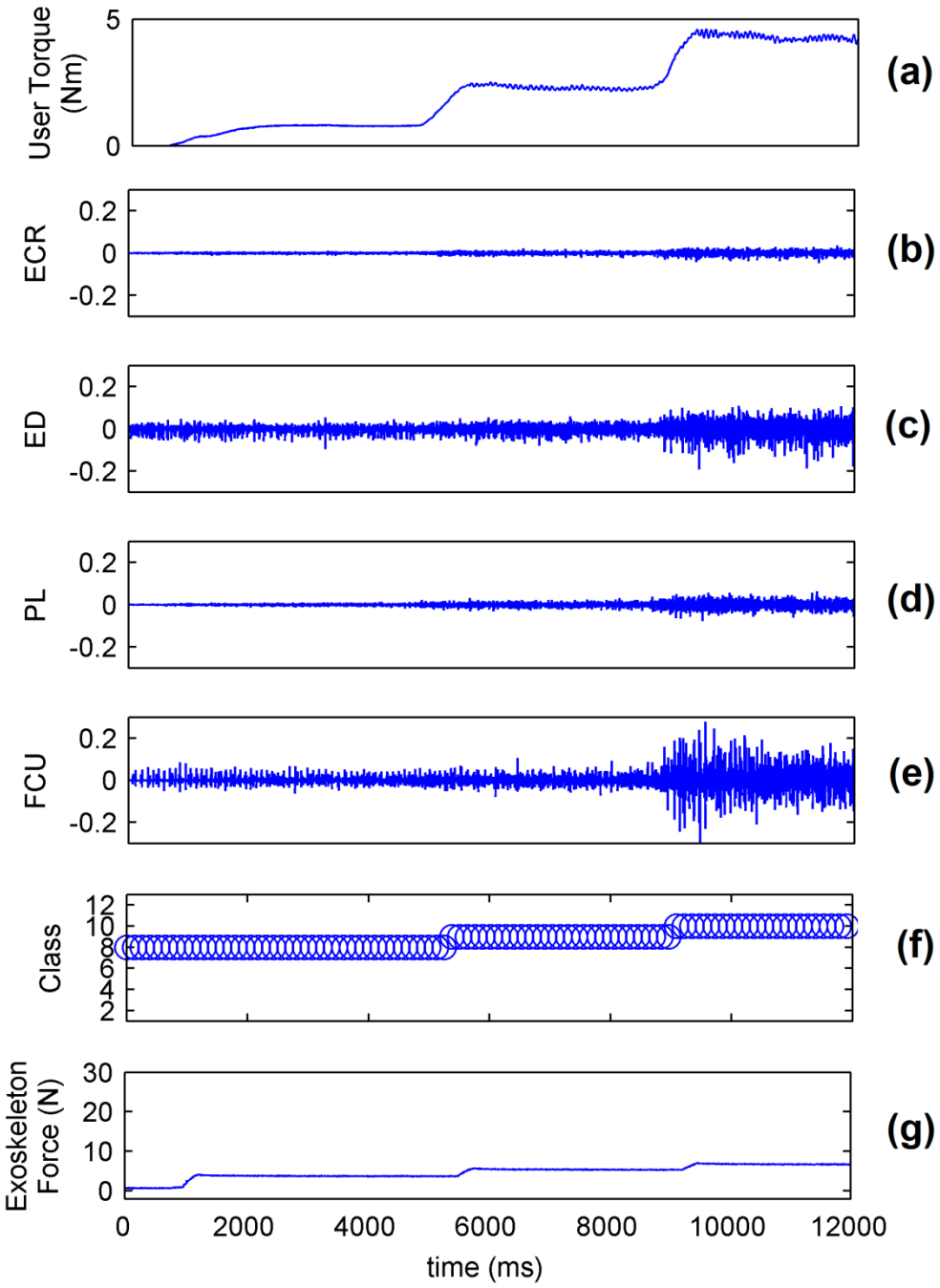

Figure 5-14: System performance for wrist radial deviation

(a) Torque applied by the wrist of volunteer; (b) ECR muscle activation; (c) ED muscle activation; (d) PL muscle activation; (e) FCU muscle activation; (f) Identified class by the system; and (g) Force applied by exoskeleton.

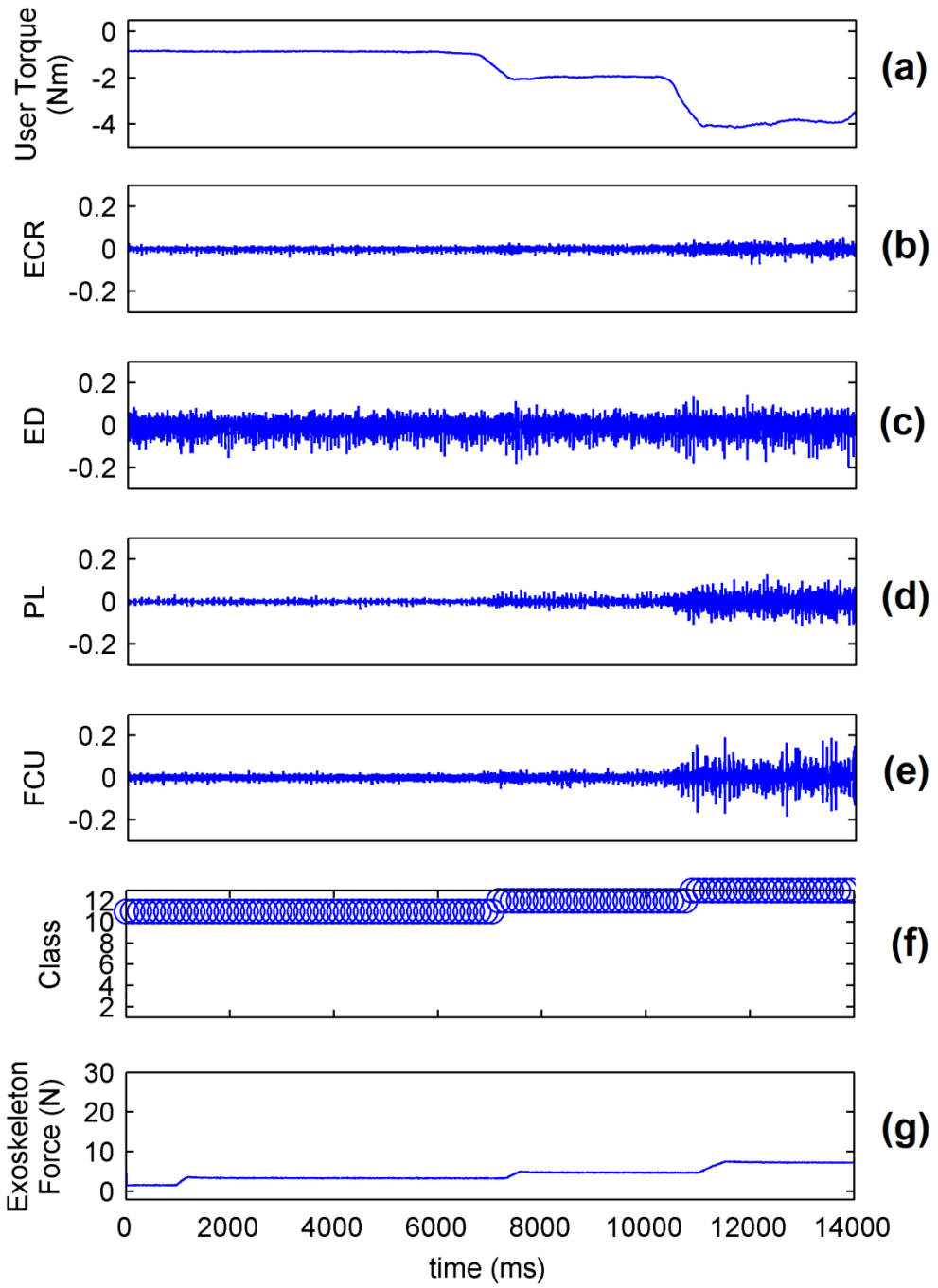

Figure 5-15: System performance for wrist ulnar deviation

(a) Torque applied by the wrist of volunteer; (b) ECR muscle activation; (c) ED muscle activation; (d) PL muscle activation; (e) FCU muscle activation; (f) Identified class by the system; and (g) Force applied by exoskeleton.

Figures 5-12, 5-13, 5-14 and 5-15 show that the classification system predicts the torque and direction of the wrist with a good accuracy. The few errors observable in the system also indicate that the misclassified points lie in the adjacent class meaning only the level of torque is incorrectly predicted and not the direction of movement. These errors can easily be catered by the mechanical delays of the system. This can be observed in Figure 5-13(f-g) where the output of the classifier shows some abnormal jumps while the output of the force sensor shows that there errors were neglected by the system producing a smooth output. It should also be noted that the delay in reaching a particular force value for the exoskeleton is due to the response time of the exoskeleton and not due to the response time of the classification system.

The results for the performance of the real-time classification system justifies the use of the proposed classification technique in practical applications such as a portable assistive device. Although the tests were conducted for isometric measurements which are not much significant in activities of daily living where the wrist is mostly in motion but in some scenarios the proposed device could potentially function where a user is stuck and is not able to move the wrist. The device can amplify the torque and can enable the user, for example, to open a tight jar or tighten screws where there is either no movement of the wrist or is very slow. In summary the idea of controlling the force along with the direction in real time using classification is feasible and can be explored for different practical applications.

CHAPTER 6 AN ASSISTIVE DEVICE: PROOF OF CONCEPT

Having developed a real-time classification and control system for the WEP, a feasibility study for its practical applicability was carried out. This chapter describes an experimental study to verify if the WEP can potentially work as an assistive device. The experimental setup and its results are discussed in the following sections.

6.1 Experimental Setup

A volunteer was asked to wear a glove (used for ensuring safety during testing), the WEP, four set of electrodes attached to the FCU, PL, ED and ECR, and to place the forearm onto a wooden platform as shown in Figure 6-1. A force sensor was attached to the bar handle of the WEP to record the isometric force during the extension of the wrist (see Figure 6-1).

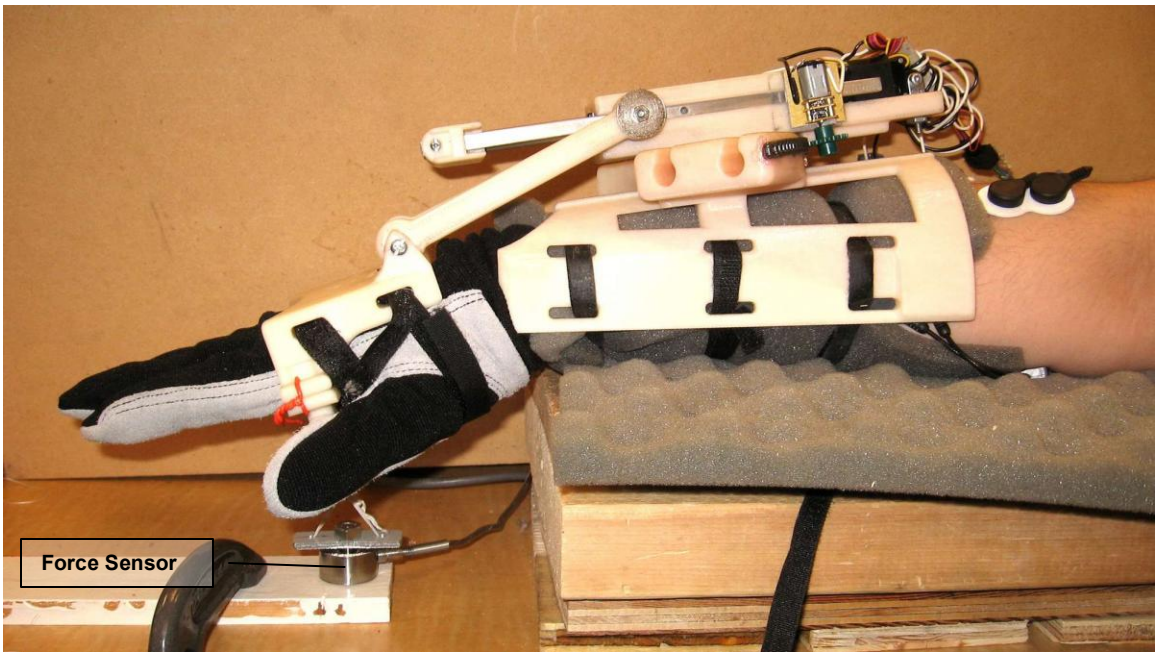

Figure 6-1: Experimental setup for assistance during wrist extension

The purpose of the test was to enable a comparison between the rms values of the sEMG with and without the WEP assistance. The overall experiment consisted of three steps: (1) training for the classification system, (2) wrist extension with assistance from the WEP and (3) wrist extension without assistance. During the training step, the parallel bars of the WEP were detached from the hand brace so that the wrist was not constrained and the force sensor could read the applied force. The classification system was then trained for four classes corresponding to rest, 10% of MVC, 20% of MVC and 30% of MVC. In the next step, the parallel bars of the WEP were attached back to the WEP to assist the wrist extension. The volunteer was asked to pull against the force sensor, and maintain a strength that corresponded to a particular class for a

short period - the WEP was expected to assist the wrist extension. In the last step, the parallel bars of the WEP were detached again from the hand brace to remove the assistance. The volunteer was subsequently asked to pull against the force sensor to a force level that was achieved with assistance, and maintain that force level for a short period of time – visual feedback of the applied force was provided to the volunteer.

6.2 Results and Discussion

Figure 6-2 shows the sEMG rms value over a period of one second for the ED muscle when applying approximately 33, 43 and 53 Newton of force in both cases in which the volunteer was and was not wearing the WEP. Figure 6-2 shows that the ED rms value was considerably less when the WED was worn, thus proving the potential assistive features of the WED and real-time classification system. It should be noted that the force level applied by the WEP can be set to be a specific percentage identified by the user - the WEP could therefore assist the user by augmenting a percentage of her/his wrist torque.

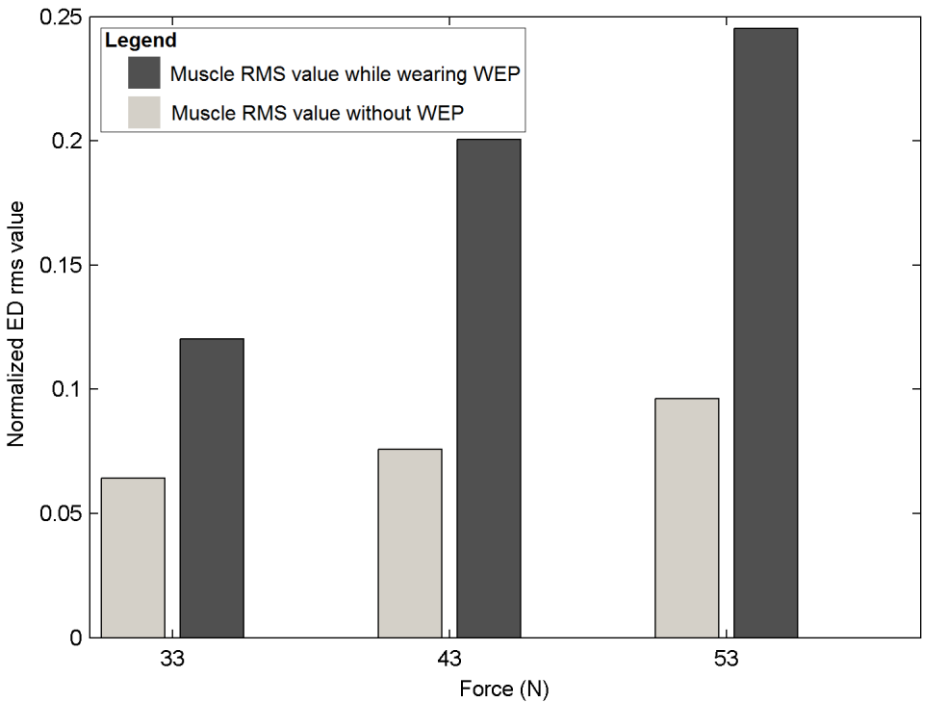

Figure 6-2: Comparison of ED rms value with and without assistance

CHAPTER 7 CONCLUSIONS AND FUTURE WORK

7.1 Thesis summary and conclusions

This thesis explores the possibility of using sEMG signals to identify the torque applied by the wrist along with direction of motion. In chapter 3, a classification method was proposed that produced reliable results for offline classification of sEMG data from four muscles of the forearm. Data was gathered from the muscles during isometric movements of the wrist by using a commercial EMG measurement system and a custom designed rig. sEMG signal rms values, AR model coefficients and waveform length were used to extract features and SVM was used to classify torque of the wrist both into 19 and 13 classes. The average accuracy for 19 classes was about 88% and for 13 classes was 96%. According to the needs of future specific applications, any number of classes in between these two could therefore be potentially suitable.

In chapter 4, some of the designs for Wrist exoskeleton prototypes (WEPs) were presented which were developed by MENRVA research group to study the performance of the classifier in real-time. The electronics and control strategies developed to derive these WEPs along with the results for their testing were also presented. The complete real-time system was presented in chapter 5 with details of the implementation and obtained results. The system was able to respond to user's intention within 250 ms proving that SVM is a suitable technique to be used in real-time sEMG recognition system.

Chapter 6 provided a proof of concept for the use of WEP as an assistive device. It was shown that the activation of the sEMG signals is reduced for the same amount of torque generated by the wrist when the user is wearing the WEP as compared to when the user produces the same torque without wearing the WEP.

7.2 Future Work

The purpose of this thesis was to develop parts of a generic assistive/rehabilitative exoskeleton. The classification system investigated in this study used isometric wrist measurements to simplify the analysis of the investigated problem. In real life scenarios, dynamic motions are required for activities of daily living. Future work will investigate the feasibility of combining force control during dynamic movements. A physics based modeling approach instead of classification is also under consideration for identifying dynamic motions.

Another important factor in the development of the device is portability. The sEMG measurement used a commercial equipment which is not portable. For portability, a compact sEMG measurement system is required. Some work to develop such a system has already been done, details of which can be found in Appendix C. However, not much testing has been done using this setup and its reliability is yet to be determined.

The real-time implementation in this study was done using LabVIEW. Although the implementation was suitable for experimental stage but for a

completely portable device, the same strategies needs to be implemented using microcontrollers. This should also improve the response time of the complete system. A wireless communication module can also be included with the final device that can communicate to a local computer and then use internet to communicate the sEMG data to a physiotherapist clinic. The configurations of the device can then be changed remotely to suite an individual user. This option can be very useful for the rehabilitative mode.

Finally all the power to the device must be supplied by some batteries to make it portable. This means that the use of power needs to be optimized. In summary, to achieve the objective of a complete wrist assistive/rehabilitative device the following tasks should be completed:

- The classification technique needs to be modified to be able to identify the torque and direction in dynamic motions.
- A portable sEMG system needs to be developed
- All the programming needs to be done on microcontrollers with wireless communication to a local terminal for any configurations or data transfers.
- All the power to the device should be supplied by batteries

APPENDICES

Appendix A: Support Vector Machines

Support Vector Machines [54] is a classification technique based on maximizing the margin between a data set and the hyper plane separating two data sets. In a general form, SVM requires solving the following optimization problem

$$\text{min} \quad \frac{1}{2}\|w\|^2 + C\sum_{n=1}^{N}\xi_n$$

$$\text{subject to} \quad \begin{matrix} \mathrm{t}_n y(\mathbf{x}_n) \geq 1-\xi_n, & n=1,...,N \\ \xi_n \geq 0 \end{matrix} \qquad (1)$$

where N is the number of data points, $\boldsymbol{x}_n$ is the vector representing a data point, t_n is the label associated with a data point, y is the learned model, $\boldsymbol{w}$ is the vector representing adaptive model parameters, ξ_n is the slack variable and $C>0$ is the penalty factor. Although SVM linearly separates two data sets, different researchers have introduced the use of kernels in the algorithm to extend it for non-linear separation without much increase in computational complexity. Some of the well-known kernels include polynomial, radial basis, Gaussian and sigmoid. SVM, which is a two class separation technique, has also been extended for multiclass classification. This is done by splitting a single multi-class problem to multiple binary classification problems. The two most common

methods are one-versus-one and one-versus-all, whose details are presented in [55]. An important property of SVM is that the model parameter estimation corresponds to a convex optimization problem meaning that any local solution will be a global optimum [55]. SVM also has a high generalization ability making it suitable for unseen data. Recently, it has been successfully applied to bio-information signals for pattern recognition [56-59].

Appendix B: Implementation as a rehabilitative device

The wrist exoskeleton prototypes (WEPs) presented in chapter 4 could also be used for rehabilitative purposes. An application in LabVIEW was developed to use the first version of WEP, which has one degree of freedom of movement, as a rehabilitation device. The application had two modes of operation; manual and auto. In manual mode, the operator could move the WEP to any position while not exceeding the force from a specified level. In auto mode, the application moves the WEP between flexion and extension in a cyclic manner with a configurable time period. The force applied by the WEP can be limited to any value during this exercise. Such an exercise could be useful for stroke patients. The WEP along with the LabVIEW application is currently under study for use with stroke patients in the Brain Behaviour Laboratory at the University of British Columbia.

Appendix C: Design of Potable sEMG System

One of the difficulties in making a rehabilitative or assistive device, that uses sEMG, is the size of the EMG measurement system. The commercial units for sEMG measurement are quite large and are not designed for portability. An attempt to overcome this difficulty was made by utilizing the pre-amplified leads of the Noraxon system and deriving it from custom electronics. The pre-amplifier design is probably the hardest part of an EMG acquisition system and using the commercial pre-amplified leads ensures that the deterioration of the quality of acquired EMG signal is minimized. The custom electronics basically consist of voltage regulators that supply +5 and -5 V to the preamplifier and obtain the output. This output is in the range of about 10-500 mV. This signal can be used directly or further amplified according to the requirements. The signal acquired by this setup seems to be quite reliable but extensive testing has not been carried out. A picture of this setup is shown in Figure C-1.

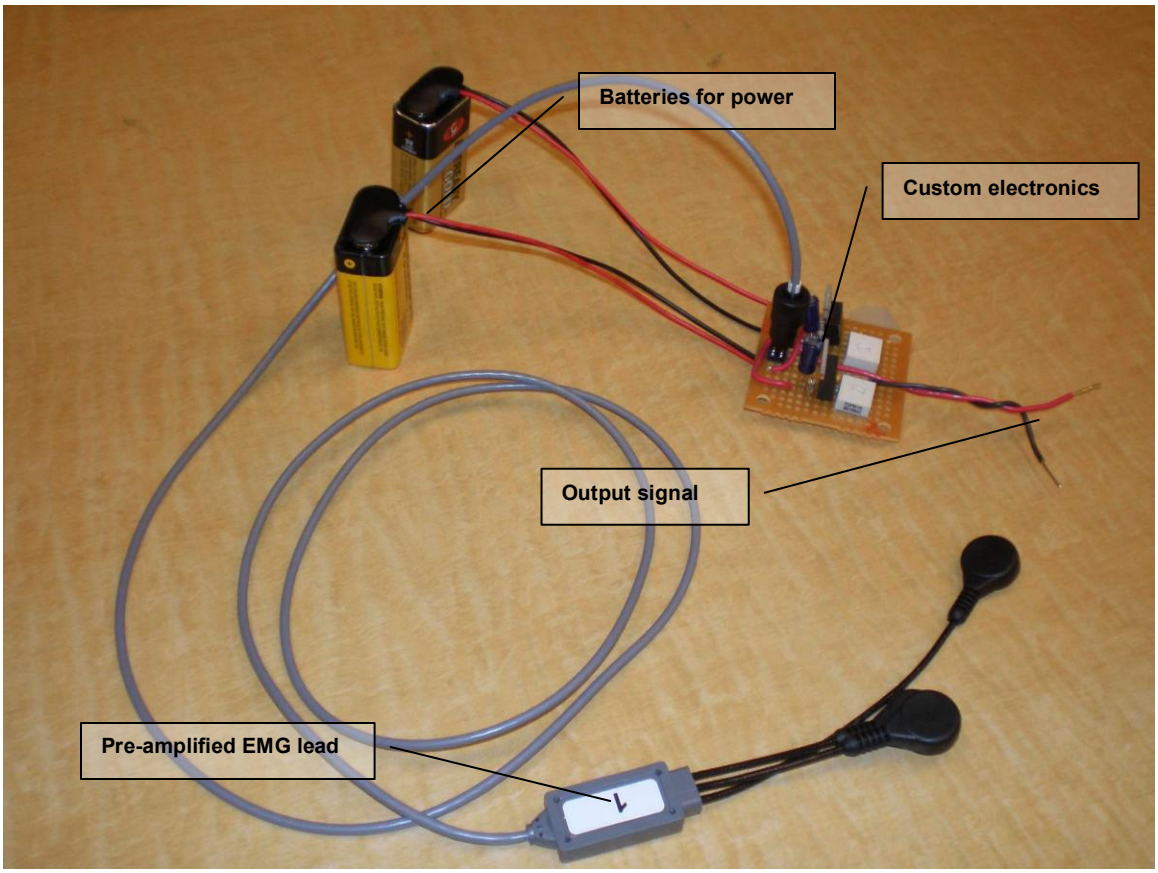

Figure C-1: Compact sEMG measurement system

Appendix D: Design of Amplifier Circuit for Force/Torque Sensors

The force and torque sensors were used for different tests performed throughout the thesis work. The output of these sensors were very small (see datasheets in Appendix F and G) and they required proper excitation voltage for normal functionality. In order to supply appropriate voltage to the sensors and amplify their output, a custom electronic board was developed. This board was capable to supply excitation voltage and amplify the output of two sensors at a time. It took input power from two DC adapters and used voltage regulators (LM317 and LM337) to supply +10 and -10 voltages to the amplifier IC (INA122P). The excitation voltage for the sensors was also set to 10 VDC. The gain of the amplifier IC was set to 430.53 so that the sensors provided an output voltage ranging from -10 to +10 V. Figure D-1 shows the schematic of the electronic board.

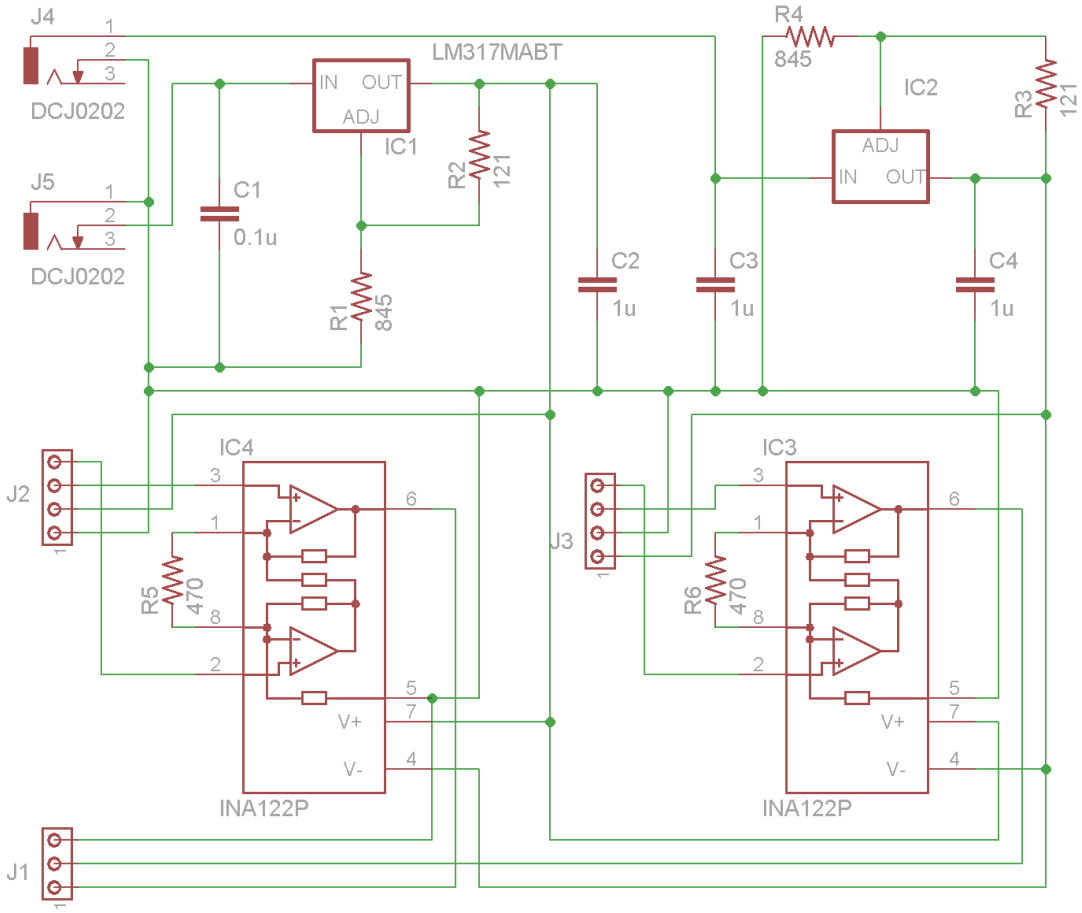

Figure D-1: Schematic of amplifier for force/torque sensors

Appendix E: Data Sheet for Firgelli Linear Actuator

The specifications for the Firgelli linear actuators are given in Table E-1 and the dimensions are shown in Figure E-1.

Table E-1: Specifications for Firgelli L12 linear actuator

	Model # L12-100-210-12-P	**Model # L12-50-210-12-P**
Parameter	**Value**	
Peak Power Point	45 N at 2.5 mm/s	45 N at 2.5 mm/s
Peak Efficiency Point	18 N at 4 mm/s	18 N at 4 mm/s
Max Speed (no load)	5 mm/s	5 mm/s
Backdrive Force	150 N	150 N
Stroke length	100 mm	50 mm
Weight	56 g	40 g
Positional Accuracy	0.3 mm	0.2 mm
Max side force (fully extended)	15 N	30 N
Mechanical Backlash	0.1 mm	0.1 mm
Feedback potentiometer	2.75 kΩ/mm±30%, 1% linearity	2.75 kΩ/mm±30%, 1% linearity
Duty cycle	20 %	20 %
Lifetime	1000 hours at rated duty cycle	1000 hours at rated duty cycle
Operating temperature	-10ºC to +50ºC	-10ºC to +50ºC
Storage temperature	-30ºC to +70ºC	-30ºC to +70ºC
Ingress protection rating	IP-54	IP-54
Audible noise	55 dB at 45 cm	55 dB at 45 cm
Operating Voltage	12 V	12 V
Stall current	200 mA	200 mA

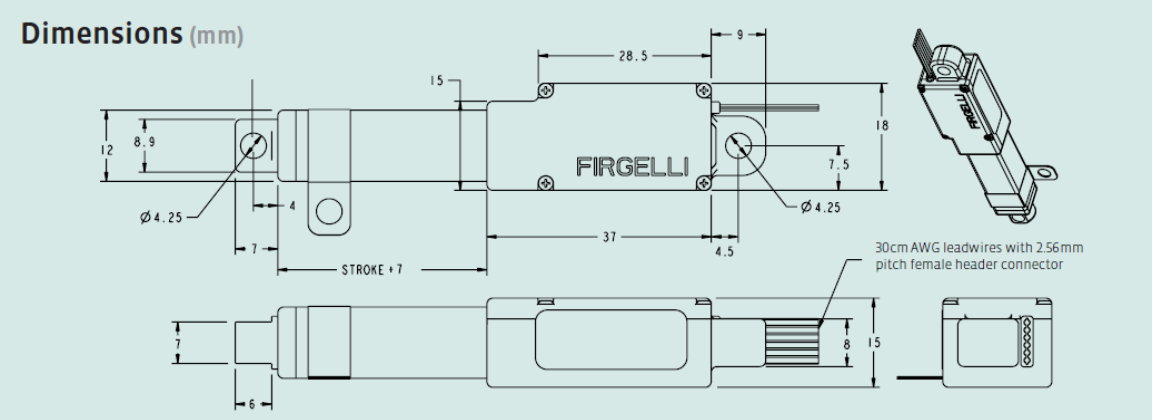

Figure E-1: Dimensions for Firgelli L12 linear actuator

Appendix F: Data Sheet for force sensor (Futek LCM-300)

The specifications for the bi-directional force sensor from Futek are shown in Table F-1 and its dimensions are shown in Figure F-1.

Table F-1: Specifications for Futek LCM-300

Parameter	Value
Rated Output (R. O.)	2mV/V nom
Safe Overload	150% of R. O.
Zero balance	±3% of R. O.
Excitation (VDC or VAC)	15 Max
Bridge resistance	700 Ω nom
Nonlinearity	±0.5% of R. O.
Hysteresis	±0.5% of R. O.
Nonrepeatability	±0.1% of R. O.
Temp. shift zero	±0.005% of R. O. /ºF
Temp. shift span	±0.02% of load /ºF
Compensated temp.	60 to 160ºF
Operating temp.	-45 to 200ºF
Weight	2 oz.
Material	17-4PH S.S
Deflection	0.001 to 0.002 nom
Cable	28 AWG, 4 conductor, spiral shielded PVC cable 10 ft long

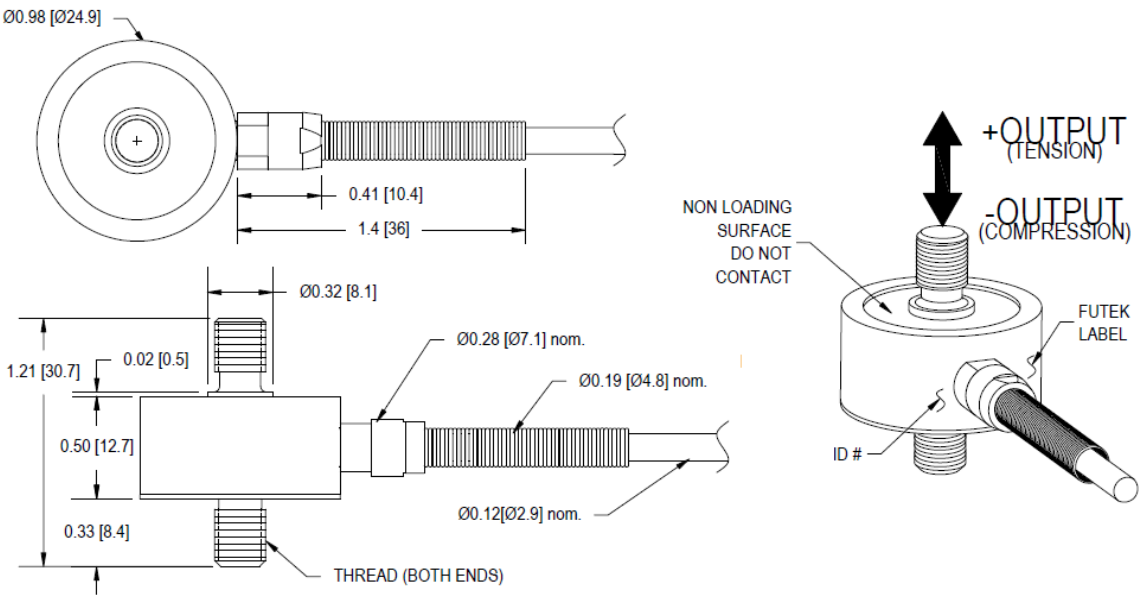

Figure F-1: Dimensions for Futek LCM-300

Appendix G: Data Sheet for torque sensor (Transducer Techniques TRT-100)

The specifications for the torque sensor from Transducer Techniques are shown in Table G-1 and its dimensions are shown in Figure G-1.

Table G-1: Specifications for Transducer Techniques TRT-100

Parameter	Value
Rated Output (R. O.)	2mV/V nom
Nonlinearity	0.1% of R. O.
Hysteresis	0.1% of R. O.
Nonrepeatability	0.05% of R. O.
Zero balance	1.0% of R. O.
Compensated temp. range	60º to 160ºF
Safe temp. range	-65º to 200ºF
Temp. effect on output	0.005% of load /ºF
Temp. effect on zero	0.005% of R. O. /ºF
Thermal resistance	350Ω nom
Excitation voltage	10 VDC
Safe overload	150% of R. O.
Capacity	100 Lbs
Torsional stiffness	10,125 In Lbs/rad
Max overhung moment	100 In Lbs
Max shear	40 Lbs
Max thrust	800 Lbs

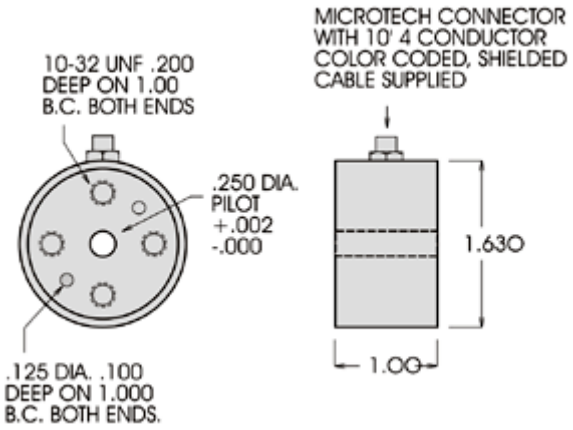

Figure G-1: Dimensions for Transducer Techniques TRT-100

Appendix H: Data Sheet for motor driver IC (L298)

The specifications for the motor driver IC L298 are shown in Table H-1 and its pin configuration is shown in Figure H-1.

Table H-1: Specifications for L298 driver IC

Symbol	Parameter	Test Conditions	Min	Typ	Max	Unit
V_S	Supply voltage (pin 4)	Operative condition	V_{IH}+ 2.5		46	V
V_{SS}	Logic supply voltage (pin 9)		4.5	5	7	V
I_{SS}	Quiescent current from V_{SS} (pin 9)	V_{en}=H;I_L=0 V_i=L V_i=H		24 7	36 12	mA mA
		V_{en}=L V_i=X			6	mA
V_{iL}	Input low voltage (pins 5, 7, 10, 12)		-0.3		1.5	V
V_{iH}	Input high voltage (pins 5, 7, 10, 12)		2.3		VSS	V
I_{iL}	Low voltage input current (pins 5, 7, 10, 12)	V_i=L			-10	µA
I_{iH}	High voltage input current (pins 5, 7, 10, 12)	V_i=H ≤ V_{SS}-0.6V		30	100	µA
V_{en}=L	Enable low voltage (pins 6, 11)		-0.3		1.5	V
V_{en}=H	Enable high voltage (pins 6, 11)		2.3		V_{SS}	V
I_{en}=L	Low voltage enable current (pins 6, 11)	V_{en}=L			-10	µA
I_{en}=H	High voltage enable current (pins 6, 11)	V_{en}=H ≤ V_{SS}-0.6V		30	100	µA
$V_{CEsat(H)}$	Source saturation voltage	I_L=1A I_L=2A	0.95	1.35 2	1.7 2.7	V V
$V_{CEsat(L)}$	Sink saturation voltage	I_L=1A (5) I_L=2A (5)	0.85	1.2 1.7	1.6 2.3	V V
V_{CEsat}	Total drop	I_L=1A (5) I_L=2A (5)	1.80		3.2 4.9	V V
V_{sens}	Sensing voltage (pins 1, 15)		-1 (1)		2	V

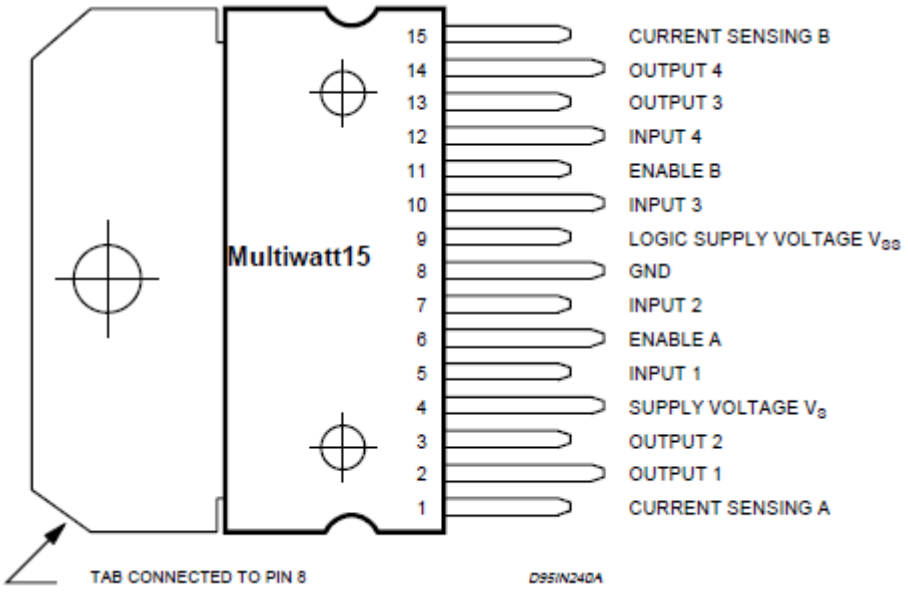

Figure H-1: Pin connections for L298 driver IC

Appendix I: Data Sheet for amplifier IC (INA122P)

The specifications for the motor driver IC L298 are shown in Table I-1 and its pin configuration is shown in Figure I-1.

Table I-1: Specifications for INA-122P

Parameter	Conditions	Min	Typ	Max	Unit
Input offset voltage			±100	±250	µV
Input impedence			10^{10}||3		Ω||pF
Safe input voltage	R_S=0 R_S=10kΩ	-0.3 -40		+0.3 +40	V V
Common-mode voltage range		0		3.4	V
Common-mode rejection	V_{CM}=0V to 3.4 V	83	96		bB
Input bias current			-10	-25	nA
Input offset current			±1	±2	nA
Gain		G=5 to 10k			
Gain equation		G=5+200kΩ/R_G			
Gain error	G=5 G=100		±0.05 ±0.3	±0.1 ±0.5	% %
Nonlinearity	G=100, V_o=-14.85 to 14.9V		±0.005	±0.012	%
Voltage noise, f=1kHz			60		nV/$\sqrt{Hz}$
Current noise, f=1kHz			80		fA/$\sqrt{Hz}$
Output short circuit current	Short-circuit to ground		+3/-30		mA
Bandwidth, -3 dB	G=5 G=500		120 0.9		kHz kHz
Slew rate			0.08/- 0.16		V/µs
Settling time, 0.01%	G=5 G=500		350 1.8		µs ms
Overload recovery	50% input overload		3		µs
Power supply range		-0.9/1.3		±18	V
Power supply current	I_o=0		60	85	µA
Operating temperature range		-55		85	ºC

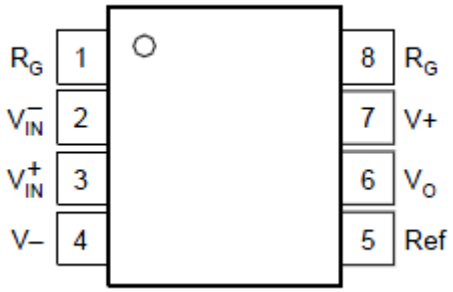

Figure I-1: Pin configuration for INA122P

Appendix J: Data Sheet for AND Gate IC (74HC08)

The specifications for the AND gate IC 74HC08 are shown in Table J-1 and its pin configuration and logic symbol are shown in Figure J-1.

Table J-1: Specifications for 74HC08

Parameter	Conditions	Min	Typ	Max	Unit
Supply voltage (V_{CC})		2	5	6	V
Input voltage (V_I)		0	-	V_{CC}	V
Output voltage		0	-	V_{CC}	V
Ambient temperature ($T_{amb)}$		-40	+25	+125	ºC
Input rise and fall times	V_{CC}=2V V_{CC}=4.5V V_{CC}=6V	- - -	- 6 -	1000 500 400	ns ns ns
Propagation delay	C_L=15 pF; V_{CC}=5V		7		ns
Input capacitance			3.5		pF
Power dissipation capacitance per gate			10		pF
Power dissipation	T_{amb}=-40 to +125ºC			750	mW
Output source or sink current (I_O)	-0.5V<V_O<V_{CC}+0.5V			±25	mA
High level input voltage	V_{CC}=2V V_{CC}=4.5V V_{CC}=6V	1.5 3.15 4.2	1.2 2.4 3.2		V V V
Low level input voltage	V_{CC}=2V V_{CC}=4.5V V_{CC}=6V		0.8 2.1 2.8	0.5 1.35 1.8	V V V
Input leakage current	V_I=V_{CC} or GND; V_{CC}=6V		0.1	±0.1	µA

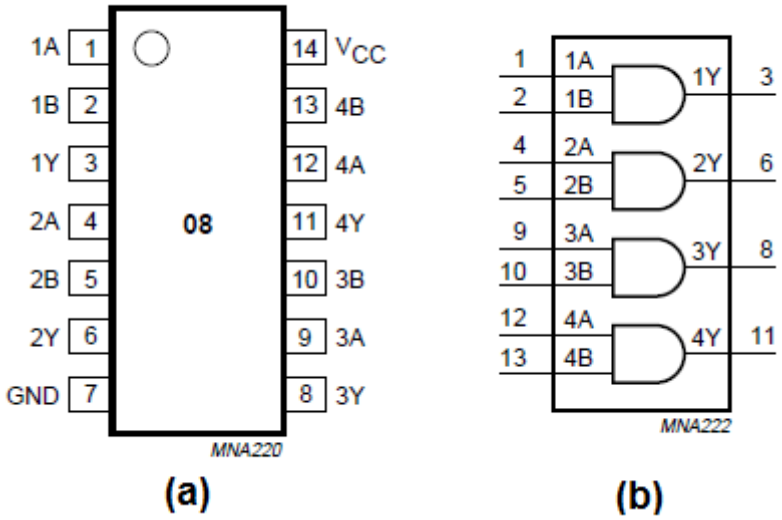

Figure J-1: Pin configuration (a) and logic symbol (b) for 74-HC-08

Appendix K: Data Sheet for voltage regulator IC (LM317)

The specifications for the AND gate IC 74HC08 are shown in Table K-1 and its pin configuration and logic symbol are shown in Figure K-1.

Table K-1: Specifications for voltage regulator LM317

Parameter	Conditions	Min	Typ	Max	Unit
Reference voltae	$3V \le (V_{IN}-V_{OUT}) \le 40V$, $10mA \le I_{OUT} \le I_{MAX}$	1.2	1.25	1.3	V
Line regulation	$3V \le (V_{IN}-V_{OUT}) \le 40V$		0.01	0.04	%/V
Load regulation	$10mA \le I_{OUT} \le I_{MAX}$		0.1	0.5	%
Thermal regulation	20 ms pulse		0.04	0.07	%/W
Adjustment pin current			50	100	µA
Adjustment pin current change	$10mA \le I_{OUT} \le I_{MAX}$, $3V \le (V_{IN}-V_{OUT}) \le 40V$		0.2	5	µA
Temperature stability	$T_{MIN} \le T_J \le T_{MAX}$		1		%
Minimum load current	$V_{IN}-V_{OUT}=40V$		3.5	10	mA
Current limit	$(V_{IN}-V_{OUT}) \le 15V$ $(V_{IN}-V_{OUT})=40V$	1.5 0.15	2.2 4	3.4	A A
RMS output noise, % of V_{OUT}	$10Hz \le f \le 10kHz$		0.003		%
Ripple rejection ratio	$V_{OUT}=10V$, f=120Hz, $C_{ADJ}=0\mu F$ $V_{OUT}=10V$, f=120Hz, $C_{ADJ}=10\mu F$	 66	65 80		dB dB
Long term stability	$T_J=125^oC$, 1000 hrs		0.3	1	%
Thermal resistance junction to case			4		$^oC/W$
Thermal resistance junction to ambient			50		$^oC/W$

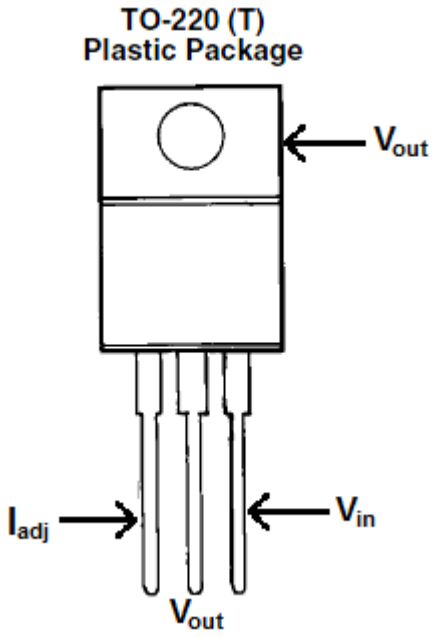

Figure K-1: Pin configuration for voltage regulator LM-317

REFERENCE LIST

[1] J.E. Morley, “The top ten hot topics in aging,” Journal of Gerontology: Medical Sciences, Vol. 59A, No. 1, pp. 24–33, 2004.

[2] D. A. Kallman, C.C. Plato, and J. D. Tobin, “The role of muscle loss in the age-related decline of grip strength: cross-sectional and longitudinal perspectives,” Journal of Gerontology, Vol. 45, pp. 82-88, 1990.

[3] T. Rantanen, K. Masaki, D. Foley, G. Izmirlian, L. White, and J. M. Guralnik, “Grip strength changes over 27 yr in Japanese-American men,” Journal of Applied Physiology, Vol. 85, pp. 2047-2053, 1998.

[4] Z. Erim, M. F. Beg, D. T. Burke, C. J. De Luca, “Effects of aging on motor-unit control properties,” Journal of Neurophysiology, Vol. 82, pp. 2081-2091, 1999.

[5] J. E. Morley, H. M. Perry, and D. K. Miller, “Something About Frailty,” Journal of Gerontology: Medical Sciences, Vol. 57A, No. 11, pp. 698–704, 2002.

[6] E. Carmeli, H. Patish, and R. Coleman, “The Aging Hand,” Journal of Gerontology: Medical Sciences, Vol. 58A, No. 2, pp. 146–152, 2003.

[7] B. K. Barry and R. G. Carson, “The Consequences of Resistance Training for Movement Control in Older Adults,” Journal of Gerontology: Medical Sciences, Vol. 59A, No. 7, pp. 730–754, 2004.

[8] A. J. Bois, G. Johnston, and D. Classen, “Spontaneous Flexor Tendon Ruptures of the Hand: Case Series and Review of the Literature,” Journal of Hand Surgery, Vol. 32A, No. 7, pp. 1061-71, 2007.

[9] S. Imai, M. Kubo, K. Kikuchi, H. Ueba, and Y. Matsusue, “Spontaneous Rupture of the Flexor Digitorum Profundus and Superficialis of the Index Finger and the Flexor Pollicis Longus Without Labor-Associated Tendon Loading, “ Journal of Hand Surgery, Vol. 29A, No. 4, pp. 587-590, 2004.

[10] F. J. T. van Oosterom, A. M. Ettema, P. G. H. Mulder, and S. E. R. Hovius, “Impairment and Disability After Severe Hand Injuries With Multiple Phalangeal Fractures, “ Journal of Hand Surgery, Vol. 32A, No. 1, pp. 91-5, 2007.

[11] http://www.heartandstroke.com/site/c.ikIQLcMWJtE/b.3483991/k.34A8/Statistics.htm.

[12] R. Riener, “Control of robots for rehabilitation,” EUROCON 2005- The International Conference on Computer as a Tool, Vol. 1, pp. 33-36, 2005.

[13] D. Reinkensmeyer, C. Pang, J. Messler, and C. Painter, “Java therapy: Web-based robotic rehabilitation: Integration of assistive technology in the information age,’’ Proceedings of 7th International Conference on Rehabilitation Robotics, pp. 66-71, April 25-27, 2001.

[14] H. Krebs, D. Williams, and N. Hogan, “Robot for wrist rehabilitation,” Proceedings of the 23rd Annual International Conference of the IEEE Engineering in Medicine and Biology Society, Vol. 2, October 2001.

[15] M. Mulas, M. Folgheraiter and G. Gini, “An EMG-controlled exoskeleton for hand rehabilitation,” Proceedings of the 2005 IEEE 9th International Conference on Rehabilitaion Robotics.

[16] B. Birch, E. Haslam, I. Heerah, N. Dechev and E. J. Park, “Design of a continuous passive and active motion device for hand rehabilitation,” 30th Annual International IEEE EMBS Conference, August 20-24, 2008.

[17] M. B. I. Reaz, M. S. Hussain and F. Mohd-Yasin, “Techniques of EMG signal analysis: detection, processing, classification and applications,” Biological Proceedings Online, Vol. 8, No. 1, pp. 11-35, 2006.

[18] Y. Y. Huang, K. H. Low and H. B. Lim, “Objective and quantitative assessment methodology of hand functions for rehabilitation,” Proceedings of 2008 IEEE International Conference on Robotics and Biomemetics, pp. 846-851, 21-26 February, 2009.

[19] O. Bai, M. Nakamura and H. Shibasaki, “Compensation of hand movement for patients by assistant force: relationship between human hand movement and robot arm motion,” IEEE Transactions on Neural Systems and Rehabilitation Engineering, Vol. 9, No. 3, pp. 302-307, 2001.

[20] G. N. Lewis and E. J. Perreault, “An assessment of robot-assisted bimanual movements on upper limb motor coordination following stroke,” IEEE Transactions on Neural Systems and Rehabilitation Engineering, Vol. 17, No. 6, pp. 595-604, 2009.

[21] P. S. Lum, C. G. Burgar, P. C. Shor, M. Majmundar and M. V. Loos, “Robot-assisted movement training compared with conventional therapy techniques for the rehabilitation of upper-limb motor function after stroke,” Archives of Physical Medicine and Rehabilitation, Vol. 83, pp. 952-959, 2002.

[22] J. Stein, K. Narenfran, J. Mcbean, K. Krebs and R. Hughes, “Electromyography-controlled exoskeleton upper-limb-powered orthosis for exercise training after stroke,” American Journal of Physical Medicine and Rehabilitation, Vol. 86, No. 4, pp. 255-261, 2007.

[23] The CyberHand project. http://www-arts.sssup.it/Cyberhand/introduction/biomechand.htm.

[24] The SmartHand project. http://www.elmat.lth.se/~smarthand/index.html.

[25] The iLimb prosthetic hand. 2007, http://www.touchbionics.com.

[26] Otto Bock Transcarpal Hand prothesis. http://www.ottobockus.com/cps/rde/xchg/ob_us_en/hs.xsl/6909.html.

[27] B. Hudgins, P. Parker and R. N. Scott, “A new strategy for multifunction myoelectric control,” IEEE Transactions on Biomedical Engineering, Vol. 40, No. 1, pp. 82-94, 1993.

[28] J. U. Chu and Y. J. Lee, “Conjugate-prior-penalized learning of Gaussian mixture models for multifunction myoelectric hand control,” IEEE Transactions on Neural Systems and Rehabilitation Engineering, Vol. 17, No. 3, pp. 287-297, 2009.

[29] J. U. Chu, I. Moon, Y. J. Lee, S. K. Kim and M. S. Mun, “A supervised feature-projection-based real-time EMG pattern recognition for multifunction myoelectric hand control,” IEEE/ASME Transactions on Mechatronics, Vol. 12, No. 3, pp. 282-290, 2007.

[30] J. U. Chu, I. Moon I and M. S. Mun, “A real-time EMG pattern recognition system based on linear-nonlinear feature projection for a multifunction myoelectric hand,” IEEE Transactions on Biomedical Engineering, Vol. 53, No. 11, pp. 2232-2239, 2006.

[31] M. Khezri and M. Jahed, “Real-time intelligent pattern recognition algorithm for surface EMG signals,” Biomedical Engineering Online, Vol. 6, No. 45, 2007.

[32] K. Englehart and B. Hudgins, “A robust, real-time control scheme for multifunction myoelectric control,” IEEE Transactions on Biomedical Engineering, Vol. 50, No. 7, pp. 848-854, 2003.

[33] F. H. Y. Chan, Y. S. Yang, F. K. Lam, Y. T. Zhang and P. A. Parker, “Fuzzy EMG classification for prosthesis control,” IEEE Transactions on Rehabilitation Engineering, Vol. 8, No. 3, pp. 305-311, 2000.

[34] B. Karlik, M. O. Tokhi and M. Alci, “A fuzzy clustering neural network architecture for multifunction upper-limb prosthesis,” IEEE Transactions on Biomedical Engineering, Vol. 50, No. 11, pp. 1255-1261, 2003.

[35] S. H. Park and S. P. Lee, “EMG pattern recognition based on artificial intelligence techniques,” IEEE Transactions on Rehabilitation Engineering, Vol. 6, No. 4, pp. 400-405, 1998.

[36] A. Soares, A. Andrade, E. Lamounier and R. Carrijo, “The development of a virtual myoelectric prosthesis controlled by an EMG pattern recognition system based on neural networks,” Journal of Intelligent Information Systems, Vol. 21, No. 2, pp. 127-141, 2003.

[37] C. Castellini and P. V. D. Smagt, “Surface EMG in advanced hand prosthetics,” Biological cybernetics. Springer-Verlag 2008.

[38] Y. H. Liu, H. P. Huang and C. H. Weng, “Recognition of electromyographic signals using cascaded kernel learning machine,” IEEE/ASME Transactions on Mechatronics, Vol. 12, No. 3, pp. 253-264, 2007.

[39] K. Englehart, B. Hudgins, P. A. Parker and M. Stevenson, “Classification of the myoelectric signal using time-frequency based representations,” Medical Engineering & Physics, Vol. 21, No. 6-7, pp. 431-438, 1999.

[40] K. Englehart, B. Hudgins and P. Parker, “A wavelet-based continuous classification scheme for multifunction myoelectric control,” IEEE Transactions on Biomedical Engineering, Vol. 48, No. 3, pp. 302-311, 2001.

[41] C. Cipriani, C. Antfolk, C. Balkenius, B. Rosen, G. Lundborg, M. C. Carrozza and F. Sebelius, “A novel concept for a prosthetic hand with a bidirectional interface: a feasibility study,” IEEE Transactions on Biomedical Engineering, Vol. 56, No. 11, pp. 2739-2743, 2009.

[42] A. D. C. Chan and K. B. Englehart, “Continuous myoelectric control for powered prosthesis using hidden markov models,” IEEE Transactions on Biomedical Engineering, Vol. 52, No. 1, pp. 121-124, 2005.

[43] S. Bitzer and P. V. D. Smagt, “Learning EMG control of a robotic hand: towards active prosthesis,” Proceedings of the IEEE International Conference on Robotics and Automation, 15-19 May, Orlando, pp. 2819-2823, 2006.

[44] M. Yoshikawa, M. Mikawa and K. Tanaka, “A Myoelectric interface for robotic hand control using support vector machine,” Proceedings of the IEEE/RSJ International Conference on Intelligent Robots and Systems, 29 October – 2 November, San Diego, pp. 2723-2728, 2007.

[45] R. N. Scott, “An introduction to myoelectric prostheses,” UNB Monographs on Myoelectric protheses, 1984.

[46] T. R. Farrell and R. F. Weir, “The optimal controller delay for myoelectric prostheses,” IEEE Transactions on Neural Systems and Rehabilitation Engineering, Vol. 15, No. 1, pp. 111-118, 2007.

[47] H. L. Lew and S. J. TSAI, “Pictorial guide to muscles and surface anatomy,” In Johnson’s practical electromyography, 4th edition, Edited by W. S. Pease, H. L. Lew and E. W. Johnson, Lippincott Williams & Wilkins, pp. 145-212, 2007.

[48] SENIAM Project. Available online at http://www.seniam.org.

[49] A. Mital and A. Pennathur, “Musculoskeletal overexertion injuries in the United States: mitigating the problem through ergonomics and engineering interventions,” Journal of Occupational Rehabilitation, Vol. 9, No. 2, pp. 115-149, 1999.

[50] H. P. Huang and C. Y. Chen, “Development of a myoelectric discrimination system for a multi-degree prosthetic hand,” Proceedings of the International Conference on Robotics and Automation, May 1999, Detroit, pp. 2392-2397, 1999.

[51] C. C. Chang and C. J. Lin, “LIBSVM: a library for support vector machines,” 2001. Software available at http://www.csie.ntu.edu.tw/ ~cjlin/libsvm.

[52] M. Henrey, C. Sheridan, Z. O. Khokhar and C. Menon, “Towards the development of a wearable rehabilitation device for stroke survivors,” Proceedings of the IEEE Toronto International Conference- Science and Technology for Humanity, 26-27 Sep.,pp. 12-17, 2009.

[53] Z. O. Khokhar, Z. G. Xiao, C. Sheridan and C. Menon, “A novel wrist rehabilitation/assistive device,” Proceeding of the IEEE 13th International Multitopic Conference, 14-15 Dec., pp.80-85, 2009.

[54] V. Vapnik, “The support vector method of function estimation,” In *Nonlinear modelling: Advanced black-box techniques,* edited by J. A. K. Sukens, J. K. Vandewalle academic publishers, Boston, 1998, pp. 55-85.

[55] C. M. Bishop, “Sparse kernel machines,” In *Pattern recognition and machine learning*, edited by M. Jordan, J. Kleinberg and B. Scholkopf, Springer, 2006, pp. 325-358.

[56] I. Guler and E. D. Ubeyli, “Multiclass support vector machines for EEG-signals classification,” IEEE Transactions on Information Technology in Biomedicine, Vol. 11, No. 2, pp. 117-126, 2007.

[57] A. H. Khandoker, M. Palaniswami and C. K. Karmakar, “Support vector machines for automated recognition of obstructive sleep apnea syndrome from ECG recordings,” IEEE Transactions on Information Technology in Biomedicine, Vol. 13, No. 1, pp. 37-48, 2009.

[58] M. A. Oskoei and H. Hu, “Support vector machine-based classification scheme for myoelectric control applied to upper limb,” IEEE Transactions on Biomedical Engineering, Vol. 55, No. 8, pp. 1956-1965, 2008.

[59] A. Kampouraki, G. Manis and C. Nikoi, “Heartbeat time series classification with support vector machines,” IEEE Transactions on Information Technology in Biomedicine, Vol. 13, No. 4, pp. 512-518, 2009.

[60] K. R. Wheeler and C. C. Jorgenson, “Gestures as input: neuroelectric joysticks and keyboards,” IEEE Pervasive Computing, Vol. 2, No. 2, pp. 56-61, 2003.

[61] H. Manabe, A. Hiraiwa and T. Sugimura, “Unvoice speech recognition using EMG-mime speech recognition,” Conference on Human Factors in Computing Systems, pp. 794-795, 2003.

[62] J. Kim, S. Mastnik and E. Andre, “EMG-based hand gesture recognition for realtime biosignal interfacing.” 12th International Conference on Intelligent User Interfaces, 13-16 Jan., pp. 30-39, 2008.